Supplementary table 1: PCR primers used in the study

	Forward	Reverse
4E-BP1	CTAGCCCTACCAGCGATGAG	CCTGGTATGAGGCCTGAATG
Atg7	GACCGGTCTTACCCTGCTC	TGTGGTTGCTTGCTTCAGAC
Atg12	CCATCCAAGGACTCATTGAC	TTGCAGTAATGCAGGACCAG
Atp5b	GAGGTCTTCACGGGTCACAT	CCCACCATGTAGAAGGCTTG
Atp5j	GGCCCAGAGTATCAGCAAGA	CTGGGGTTTGTCGATGACTT
Atp5l	CCTGCTGAAATCCCTACAGC	CACCAAACCATTCAGCACAG
Atp5o	GCTTCCTGAGTCCAAACCAA	GCCTTGCTGAGCTTCTGAAT
Atrogin 1	CAGCTGGATTGGAAGAAGATG	TCAGAACTTGAACAAATTGA
Btg1	CGGTGTCCTTCATCTCCAAG	GGTAACCTGATCCCTTGCAC
Catalase	GGACGCTCAGCTTTTCATTC	CAGGTTAGCTTTTCCCTTCG
Cathepsin L	GTTGGTGGGCTATGGCTATG	CCGGTCTTTGGCTATTTTGA
Coq2	CTGTCCCCTACTACGCTGCT	CGGTTGGAGGTGAACTTGTC
Cox4il	GGCACCAATGAATGGAAGAC	CCTTCATGTCCAGCATTCG
Cox5b	GATGAGGAGCAGGCTACTGG	CAGCCAAAACCAGATGACAG
Cox6a2	GACCTTTGTGCTGGCTCTTC	ATTGTGGAAAAGCGTGTGGT
Cyclin G2	TTCCTGAGCTGCCCACTATC	GGTGGAAAGCACAGTGTCTG
Ddb1	CCCTAAGATGCAGGAGGTTG	CGAGTTAGCTCCTCCACGAC
Fgf21	CAGGGGTCATTCAAATCCTG	GGAGTCCTTCTGAGGCAGAC
Fndc5	GGTGCTGATCATTGTTGTGG	CGCTCTTGGTTTTCTCCTTG
FoxO1	GAGAGCTCAGCCGAGAAGAG	CTCCCTCTGGATTGAGCATC
G6Pase	CTGTCTGTCCCGGATCTACC	GTAGAATCCAAGCGCGAAAC
Gadd45	GCGAGAACGACATCAACATC	TCCCGGCAAAAACAAATAAG
HPRT	CCGAGGATTTGGAAAAAGTG	CCAGCAGGTCAGCAAAGAAC
MHC1 (Myh7)	GCCAACTATGCTGGAGCTGATGCCC	GGTGCGTGGAGCGCAAGTTTGTCATAAG
MHCIIX	GAAGAGTGATTGATCCAAGTG	TATCTCCCAAAGTTATGAGTACA
Myh4	GCAGGACTTGGTGGACAAAC	CAGCTTGTTGACCTGGGACT
MuRF1	GCAAGGCTTTGAGAACATGG	TCTTCCTCATCAGCCTCCTC
Ndufb2	CAGGTGATCCAGGGTGAGTT	CTCGTCATCAGGAGGGATTC
Ndufb5	GCTTGCAGAAATCCCAGAAG	GGATAGCCAGGGTTTTCTCG
Ndufs1	GTTCTTGCTGACCCACTCGT	GCATATGGACGGCTCCTCTA
p21	CTTGTCGCTGTCTTGCACTC	CTCCTGACCCACAGCAGAAG
p27	GTGGACCAAATGCCTGACTC	CTGTTGGCCCTTTTGTTTTG
p62	GAAGCTGCCCTATACCCACA	GAGAAACCCATGGACAGCAT
Pck1	GAAGTTCGTGGAAGGCAATG	CATCTCGAGGGTCAGTGAGAG
Pgc1α	TTACACCTGTGACGCTTTCG	AGCAGGGTCAAAATCGTCTG
PPIA	GACCAAACACAAACGGTTCC	CATGCCTTCTTTCACCTTCC
SdhA	CAGTTTCGAGGCTTCTTCG	CTCAGAAAGGCCAAATGCAG
SdhB	GACGTCAGGAGCCAAAATG	CACCTCGTACGTCTGCATTC
SirT4	GAAAGAGGCGGACTCCCTAC	CGGGTCTATTAAAGGCAGCA
Sod2	CCGAGGAGAAGTACCACGAG	GCTTGATAGCCTCCAGCAAC
Tnni1 (troponin I type 1-skeletal, slow)	CTGGGCTCTAAGCACAAGGT	ATGCCAGACATAGCCTCCAC

Tnni2 (troponin I type 2- skeletal, fast)	CCTGAAGCAGGTCAAGAAGG	TCCATGCCAGACTTCTCCTC
UCP1	GCCTGGCAGATATCATCACC	CAGACCGCTGTACAGTTTCG
UCP2	GCCACTTCACTTCTGCCTTC	CTACGTTCCAGGATCCCAAG
UCP3	GCTGAAGATGGTGGCTCAG	TTAAGGCCCTCTTCAGTTGC
Uqcrc1	GAAGACATTGGTCGCAGTCTC	CGGTTGTAGTCTGGGAGCTG

Supplementary Figure Legends:

Supplemental Figure S1

Generation skeletal muscle or adipose tissue-specific *4E-BP1* transgenic mice**. (A)** Structure of *4EBP1mt* transgenic alleles. The expression of each transgene is blocked by the presence of a *loxP*-flanked translational STOP codon cassette. CRE-mediated recombination excises the STOP element, which is fused with GFP, and permits the expression of transgenes under the control of the chicken β –actin promoter, indicated by the blue line. **(B)** Expression of total 4E-BP1 protein in quadriceps muscle and **(C)** in visceral fat and liver from 6 month-old control and *Tg-4EBP1mt-muscle* male mice fed a normal chow. **(D)** Western blots on visceral fat of *Tg-4EBP1mt-fat* mice and control littermates to quantify total 4E-BP1 expression. **(E)** RT- PCR quantification of endogenous *4E-BP1* mRNA expression in quadriceps muscle from 6 month-old control and *Tg-4EBP1mt-muscle* male mice. P values were calculated by one-tailed unpaired student's t-test. RT-PCR samples were from n=4/genotype.

Supplemental Figure S2

Transgenic 4E-BP1mt protein is functional to sequester eIF4E from eIF4G. **(A)** Lysate from skeletal muscle was subjected to co-immunoprecipitate using anti-eIF4E antibody or Rabbit IgG. Western blot analysis of 4E-BP1 to detect the interaction of eIF4E and 4E-BP1. **(B)** Western blot of cap binding assay to analyze eIF4E-eIF4G complex formation in skeletal muscle. The translation initiation complex was pull down by the cap analog m^7GTP-sepharose and western blotted with antibodies against eIF4G, eIF4E, or 4E-BP1. **(C)** Quantification of cap binding assays on eIF4G level, which associated with translation initiation complex normalized to control. **(D)** Quantification of cap binding assays on eIF4G level normalized to input eIF4G level and to control. **(E)** Coomassie blue staining for total protein loading quantification and **(F)** western blot analysis of puromycin incorporation in total protein in quadriceps muscle from 6 month-old male mice injected with puromycin. **(G)** Quantification of signal from (F). P values were calculated by one-tailed unpaired student's t-test. Number of mice analyzed indicated in bar.

Supplemental Figure S3

The expression of *FoxO1* is increased in 4E-BP1 activated skeletal muscle. **(A)** Western blots and **(B)** RT-PCR quantification of *FoxO1* expression in 4E-BP1 activated mouse quadriceps

muscle from 6 month-old male mice fed a normal chow (n=4/ genotype). P values were calculated by one-tailed unpaired student's t-test. RT-PCR samples were from n=4/genotype.

Supplemental Figure S4

Initial characterization of *4E-BP1* double transgenic mice. **(A)** Body weight measurement in female mice of muscle- and adipose-specific induced *4E-BP1* transgene fed a normal chow. (n= 8-16/ genotype). **(B)** Food consumption per day and **(C)** food consumption measured in **(B)** normalized in body weight in 6 month-old male mice fed a normal chow. **(D)** IGF-1 plasma values in 6 month-old mice. Number of mice analyzed indicated in bar. P values were calculated by one-tailed unpaired Student's *t*-test.

Supplemental Figure S5

Assessment of glucose homeostasis in *4E-BP1* transgenic mice. **(A)** Fasting glucose level in 2 month-old mice. *P* vales were assessed by a two-way ANOVA. Bonferroni post-tests to compare replicate means by row. Number of mice analyzed indicated in bar. **(B)** Glucose tolerance assay in 6 month-old male and **(C)** female mice fed a normal chow. **(D)** Insulin challenge assay in 6 month-old mice male and **(E)** female mice fed a normal chow. (n=8-16/ genotype) *P* values were calculated by one-tailed unpaired Student's *t*-test.

Supplemental Figure S6

Measurement of fat mass and organ weight in 6 month-old *4E-BP1* transgenic mice fed a normal chow. **(A)** Body weight measurement, and **(B)** fat mass measurement quantified by qMR. Number of mice analyzed indicated in bar. **(C)** Organ weight normalized by total body weight in male and **(D)** female mice, (n=4/ genotype). *P* vales were assessed by a two-way ANOVA. Bonferroni post-tests to compare replicate means by row.

Supplemental Figure S7

Analysis of adipose cell size in *Tg-4EBP1mt-muscle* mice. **(A)** Quantification of adipose size in visceral fat and **(B)** inguinal fat from 6 month-old male mice fed a normal chow. (n=3-4 /genotype).

Supplemental Figure S8

Characterization of adipose tissue in *Tg-4EBP1mt-muscle* mice. **(A)** RT-PCR quantification of *Pgc-1α* and **(B)** *Ucp1* in 6 month-old male mouse adipose tissues (n=4/ genotype). *P* vales were assessed by a two-way ANOVA. Bonferroni post-tests to compare replicate means by row. RT-PCR samples were from n=4/genotype. **(C)** Representative Western blots analysis of CPT1α and UCP1 expression in brown adipose tissue from 6 month-old male mice fed a normal chow.

Supplemental Figure S9

Measurement of lean mass in 6 month-old control and *Tg-4EBP1mt-muscle* mice. **(A)** Lean mass measurement in male and **(B)** female mice quantified by qMR (each dot represents an individual mouse).

Supplemental Figure S10

Activation of 4E-BP1 in skeletal muscles leads to muscular atrophy. **(A)** Representative images of Hematoxylin & Eosin staining to show morphology, Trichrome staining to detect fibrosis, Periodic acid-Schiff staining to detect glycogen deposit, and Oil-Red staining to detect lipid accumulation in male mouse quadriceps muscle sections from 6 month-old male mice fed a normal chow. Scale bar = 100μm. **(B)** Quantification of muscle fiber size in 6 month-old male and **(C)** female mouse quadriceps muscle. **(D)** Analysis of the mean fiber cross-section-area in quadriceps muscles from (A) and (B). **(E)** Quantification of percentage of central nuclei in 6 month-old mouse quadriceps muscles. (Normal chow fed mice were used in the assessments.) *P* vales were assessed by a two-way ANOVA. Bonferroni post-tests to compare replicate means by row. Number of mice analyzed indicated in bar.

Supplemental Figure S11

Autophagy is induced in *Tg-4EBP1mt-muscle* mouse muscle. **(A)** Real-Time PCR quantification of atrophic and autophagy-related genes in male quadriceps muscle from 6 month-old mice fed a normal chow (n=4/ genotype). *P* vales were assessed by a two-way ANOVA. Bonferroni post-tests to compare replicate means by row. RT-PCR samples were from n=4/genotype. **(B)** Western blots on quadriceps muscles from 12 month-old male mice fed a normal chow to detect increased autophagy-induced LC3 II isoform. **(C)** Quantification of ration of LC3-II and LC3-I signaling from (B). *P* values were calculated by one-tailed unpaired Student's *t*-test. *P<0.05; **P<0.01

Supplemental Figure S12

Activity assessment in *Tg-4EBP1mt-muscle* mice. **(A)** Running capacity measured by treadmill in male and **(B)** female mice. **(C)** Volunteer activities assay, which is monitored in metabolic cage by assessment of the travel distance that a single-housed mouse moved around the cage in 6 month-old male and **(D)** female mice. (Normal chow fed mice were used in the assessments. n=5-8 /genotype). *P* vales were assessed by a two-way ANOVA. Bonferroni post-tests to compare replicate means by row.

Supplemental Figure S13

PI3Kinase signaling is altered in 4E-BP1 activated skeletal muscle. **(A)** Western blots of AKT1 expression. **(B)** RT-PCR quantification of FOXO1 target genes. n=4/ genotype. *P* vales were assessed by a two-way ANOVA. Bonferroni post-tests to compare replicate means by row. **P<0.005; ***P<0.001

Supplemental Figure S14

Measurement of total body fat mass in 6 month-old control and *Tg-4EBP1mt-muscle* mice. **(A)** Fat mass measurement in male and **(B)** female mice quantified by qMR (each dot represents an individual mouse). **(C)** Serum leptin measurement in 2-month-old mice fed a normal chow (number of mice analyzed indicated in bar). *P* vales were assessed by a two-way ANOVA. Bonferroni post-tests to compare replicate means by row.

Supplemental Figure S15

Assessment of fat metabolism in in control and *Tg-4EBP1mt-muscle* mice. **(A)** Cholesterol, **(B)** free fatty acid, and **(C)** triglyceride plasma values in 6-month-old mice. *P* vales were assessed by a two-way ANOVA. Bonferroni post-tests to compare replicate means by row. Number of mice analyzed indicated in bar.

Supplemental Figure S16

Activated 4E-BP1 in skeletal muscles leads to muscle fiber type transformation. **(A)** Representative images of immunofluorescence stained tibias anterior and quadriceps muscle sections from 6 month-old male mice fed a normal chow to detect each muscle type. Type I muscle (MHCI-blue) and type II muscle (MHC2a-green, MHC2b-red and MHC2x-unstained). Scale bar = 100μm. **(B)** RT-PCR quantification of slow (*Tnni1*) and fast (*Tnni2*) genes, **(C)** of

myosin heavy chain 1(*Mhc1*) for detecting type I muscle and myosin heavy chain 4 (*Myh4*) for detecting type IIb muscle, and **(D)** of myosin heavy chain IIx (MyhcIIx) for detecting type IIx muscle in quadriceps muscle from 6-month-old male mice fed a normal chow. **(E)** RT-PCR quantification of mtDNA (*CoxII*) and nuclear genomic DNA (*β-actin*) in indicated tissues from 6-month-old male mice fed a normal chow. *P* vales were assessed by a two-way ANOVA. Bonferroni post-tests to compare replicate means by row. (n=4/ genotype)

Supplemental Figure S17

Increased uncouple protein expression in *Tg-4EBP1mt-muscle* mouse skeletal muscle. **(A)** Real-Time PCR quantification of PGC-1α target genes in quadriceps muscle from 6-month-old male mice fed a normal chow. (n=4/ genotype) *P* vales were assessed by a two-way ANOVA. Bonferroni post-tests to compare replicate means by row. *P<0.05; ***P<0.001. **(B)** Western blots of UCP3 in quadriceps muscles.

Supplemental Figure S18

Increased metabolic rate and mitochondria activity in *Tg-4EBP1mt-muscle* mice**. (A)** Oxygen consumption measurement in 6 month-old female mice fed a normal chow (n=8/ genotype). (B) Respiratory quotient (RQ) quantified by oxygen consumption and CO2 generation in 6 month-old mice fed a normal chow (n=5-10/ genotype). **(C)** Oxygen consumption rates (OCR) measured in isolated skeletal muscle mitochondria in the presence of Pyruvate/Malate and **(D)** Palmitoyl Carnitine /Malate (n=5/ genotype). *P* vales were assessed by a two-way ANOVA. Bonferroni post-tests to compare replicate means by row.

Supplemental Figure S19

HFD induces weight gain in *4E-BP1* transgenic mice comparable to control mice. **(A)** Body weight measurement in male and **(B)** female of *4E-BP1* transgenic line and control mice fed a HFD. (n= 8-16/genotype).

Supplemental Figure S20

Assessment of glucose homeostasis in mice fed a HFD. **(A)** Body weight and **(B)** Insulin plasma values at 6-month-old mice fed HFD. *P* vales were assessed by a two-way ANOVA. Bonferroni post-tests to compare replicate means by row. Number of mice analyzed indicated in bar. **(C)** Glucose tolerance assay and **(D)** insulin challenge assay in 6 hr-fasted female mice fed a HFD at

6 months of age (n=8-24/ genotype). *P<0.05; ***P<0.001; *P* values were calculated by one-tailed unpaired Student's *t*-test.

Supplemental Figure S21

Increased insulin sensitivity in *Tg-4EBP1mt-muscle* mice fed a HFD. Western blot of AKT1 phosphorylation at Ser 473 and total AKT1 detected in liver and visceral fat of male mice before(-) or after(+) insulin injection on a HFD feeding.

Supplemental Figure S22

Quantification of obesity in *4E-BP1* transgenic mice on HFD. **(A)** Total fat mass measurement quantified by qMR in mice on a HFD feeding. **(B)** Normalized the analysis of (A) with body weight. *P* vales were assessed by a two-way ANOVA. Bonferroni post-tests to compare replicate means by row. Number of mice analyzed indicated in bar.

Supplemental Figure S23

Uncoupling protein 1 expression is increased in *Tg-4EBP1mt-muscle* mouse brown adipose tissue. Real-time PCR quantification of *Ucp1* expression in brown adipose tissues from 6 month-old male mice fed a normal chow or HFD (n=4/ genotype and diet). *P* vales were assessed by a two-way ANOVA. Bonferroni post-tests to compare replicate means by row.

Supplemental Figure S24

Measurement of metabolic rates in *Tg-4EBP1mt-muscle* mice on a HFD. (A) Oxygen consumption measurement in 6-month-old mice fed a HFD in 3 day-night period of time (n=8/genotype). (B) RQ quantified by oxygen consumption and CO2 generation in 6 month-old mice fed a HFD (n=4-6/ genotype). *P* vales were assessed by a two-way ANOVA. Bonferroni post-tests to compare replicate means by row.

Supplemental Figure S25

Assessment of uncoupling protein expression in 4E-BP1 activated skeletal muscles. **(A)** Real-time RT-PCR quantification of *Ucp2* and **(B)** *Ucp3* expression in quadriceps muscle from 6 month-old male control and *Tg-4EBP1mt-muscle* mice fed a normal chow or HFD. *P* vales were assessed by a two-way ANOVA. Bonferroni post-tests to compare replicate means by row. (n=4/ genotype)

Supplemental Figure S26

Assessments of behavior in *Tg-4EBP1mt-muscle* mice on a HFD. **(A)** Food intake and **(B)** measurement of voluntary home-cage activity in 6-month-old mice fed a HFD in 3 day-night period of time (n=8/genotype). *P* vales were assessed by a two-way ANOVA. Bonferroni post-tests to compare replicate means by row.

Supplemental Figure S27

Activation of 4E-BP1 in skeletal muscles slows aging-induced muscular atrophy. Quantification of muscle fiber size in 6 and 17 month-old mouse quadriceps muscle. (Normal chow fed mice were used in the assessments. n=3-5/ genotype)

Supplemental Figure S28

Tg-4EBP1mt-muscle mice is resistant to aging-induced obesity. **(A)** Body weight, **(B)** lean mass, **(C)** lean mass percentage measured in **(B)** normalized in body weight, **(D)** total fat mass, and **(E)** fat mass percentage measured in **(D)** normalized in body weight measurement quantified by qMR in normal chow fed male mice. *P* vales were assessed by a two-way ANOVA. Bonferroni post-tests to compare replicate means by row. Number of mice analyzed indicated in bar.

Supplemental Figure S29

Measurement of respiratory quotient in *Tg-4EBP1mt-muscle* mice during aging. (A) and (B) RQ quantified by oxygen consumption and CO2 generation in normal diet fed male mice (n=5-13/ genotype). *P* vales were assessed by a two-way ANOVA. Bonferroni post-tests to compare replicate means by row.

Supplemental Figure S30

Increased FGF-21 expression from 4EBP1 activated skeletal muscle reduced lipogensis in *Tg-4EBP1mt-muscle* mouse liver. **(A)** Western blot on quadriceps muscles from 6 month-old female mice fed a normal chow to detect FGF-21 expression. **(B)** Western blots on quadriceps muscles from 6 month-old male mice fed a normal chow to detect SREBP1 expression in liver. **(C)** RT-PCR quantification of genes involved in fatty acid metabolism in liver (n=4/ genotype). *P* vales were assessed by a two-way ANOVA. Bonferroni post-tests to compare replicate means by row. *P<0.05; **P<0.01; ***P<0.001.

Supplemental Figure S31

Analysis of β–oxidation gene expression in *Tg-4EBP1mt-muscle* mice. **(A)** RT-PCR quantification of β–oxidation gene expression in 6 month-old normal diet fed male mouse skeletal muscle, and **(B)** visceral fat. **(C)** RT-PCR quantification of *Fgf-21* expression in 6 month-old HFD fed male mouse skeletal muscle. **(D)** RT-PCR quantification of β–oxidation gene expression in 6 month-old HFD fed male mouse skeletal muscle, **(E)** visceral fat, and **(F)** liver. *P* vales were assessed by a two-way ANOVA. Bonferroni post-tests to compare replicate means by row. (n=4/ genotype)

Supplemental Figure S32

Acute activated 4E-BP1 in skeletal muscles leads to increased *Fgf-21* and muscle type I gene expression. **(A)** RT-PCR quantification of slow (*Tnni1*) and fast (*Tnni2*) genes, **(B)** of myosin heavy chain 1(*Mhc1*) for detecting type I muscle and myosin heavy chain 4 (*Myh4*) for detecting type IIb muscle, and (C) of myosin heavy chain IIx (MyhcIIx) for detecting type IIx muscle in quadriceps muscle. *P* vales were assessed by a two-way ANOVA. Bonferroni post-tests to compare replicate means by row. (D) RT-PCR quantification of mtDNA (*CoxII*) and nuclear genomic DNA (*β-actin*). **(E)** RT-PCR quantification of *Fgf21* in quadriceps muscle. *P* values were calculated by two-tailed unpaired Student's *t*-test. Mice were injected with either Tamoxifen or Oil at 6 month of age for 5 days and harvested 2 days after the final injections. (n=3-5/group)

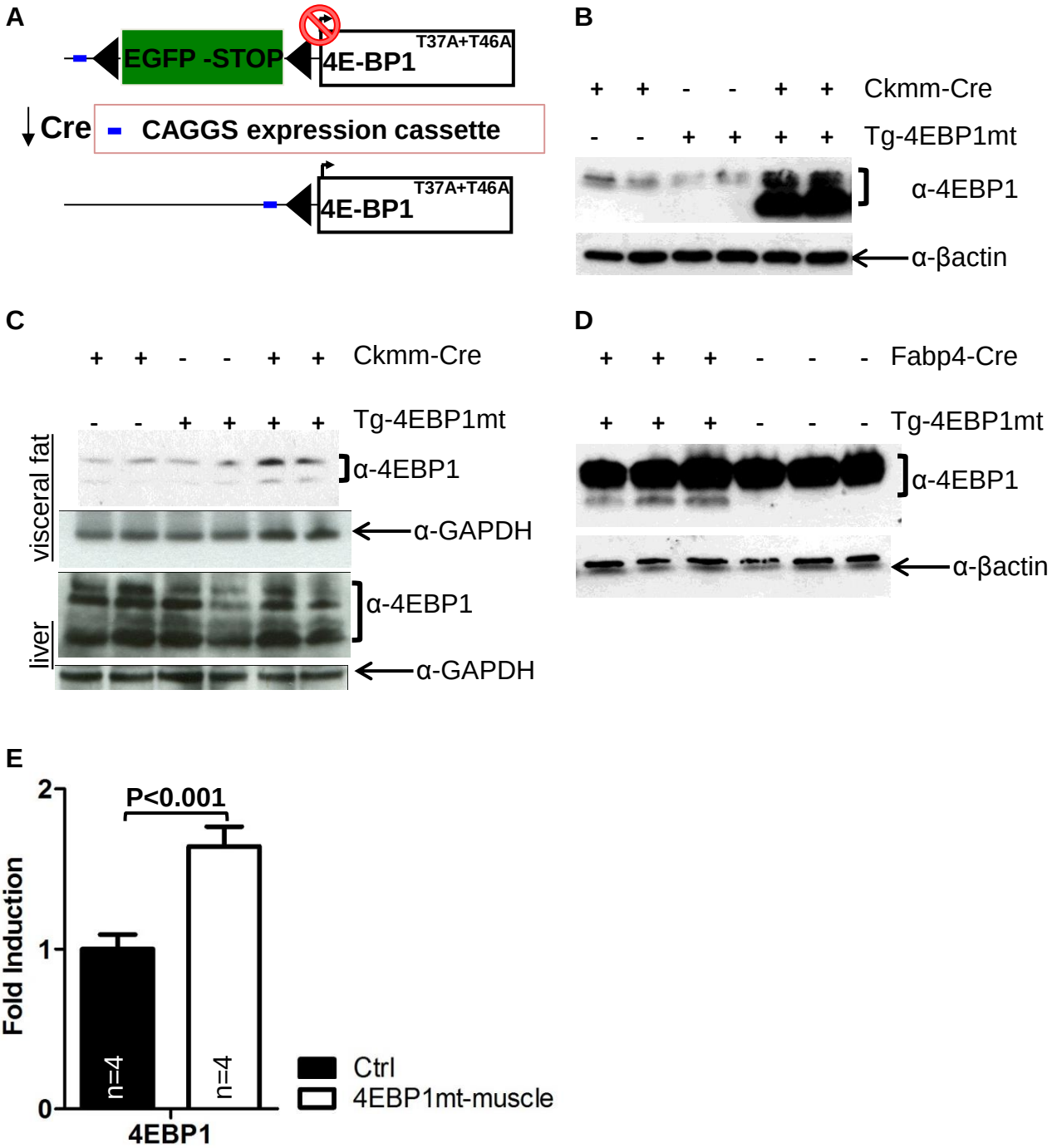

Supplementary Figure 1.

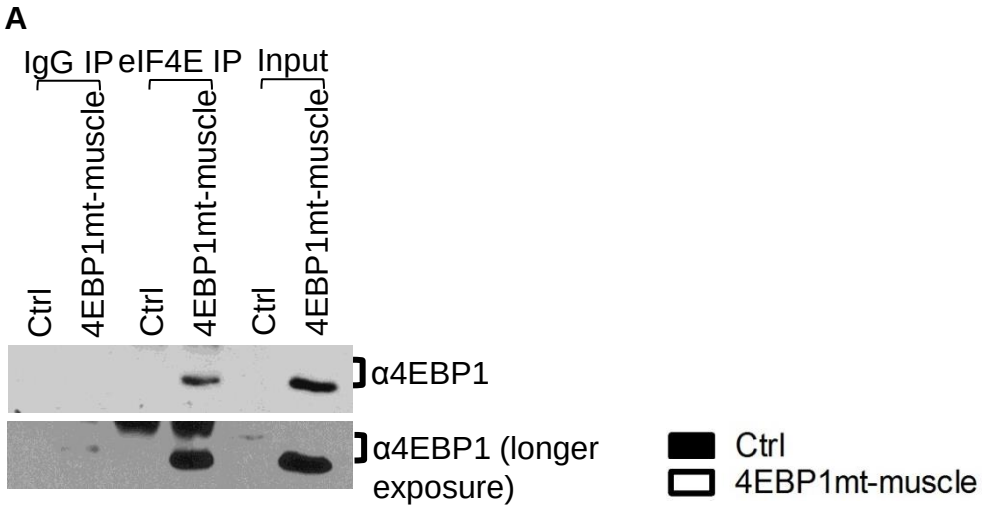

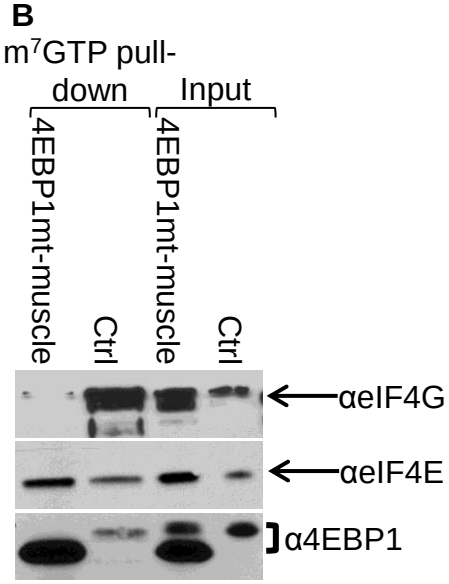

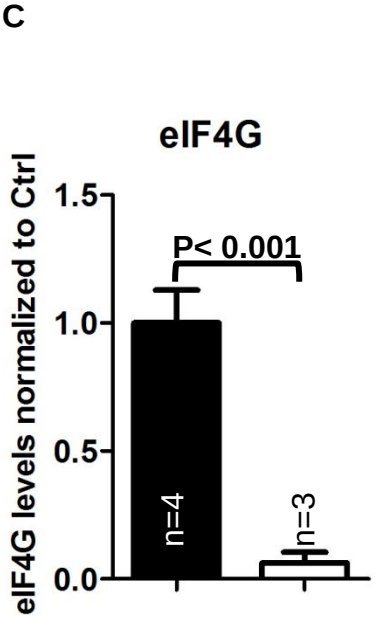

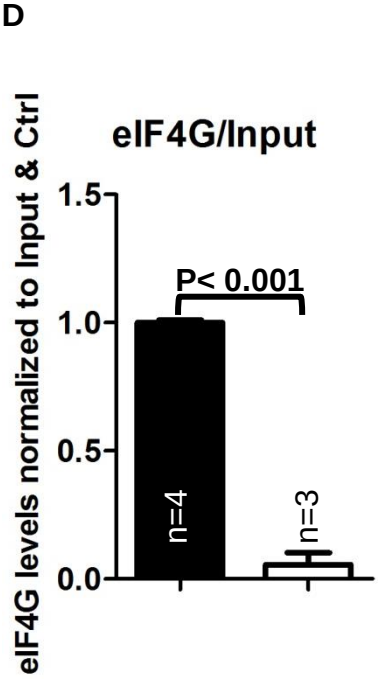

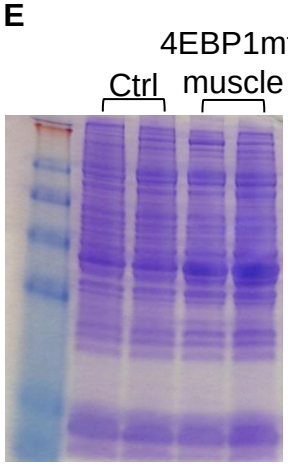

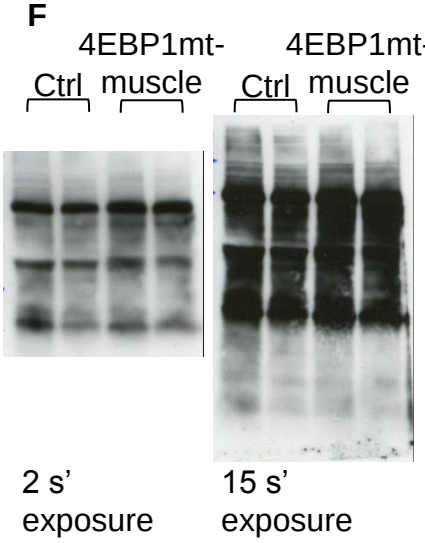

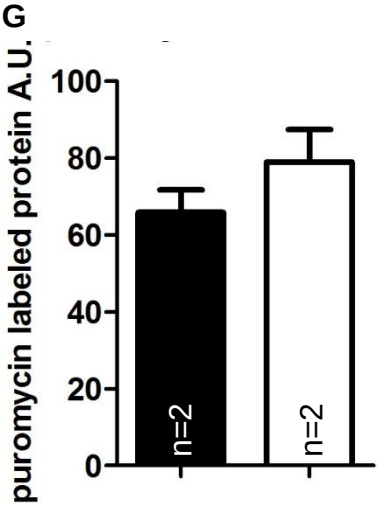

Supplementary Figure 2.

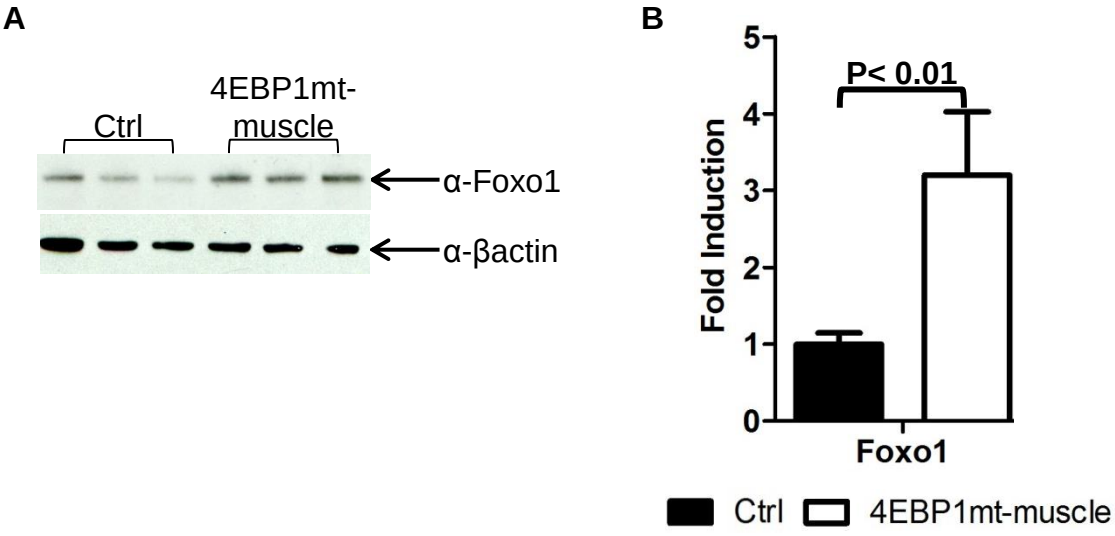

Supplementary Figure 3.

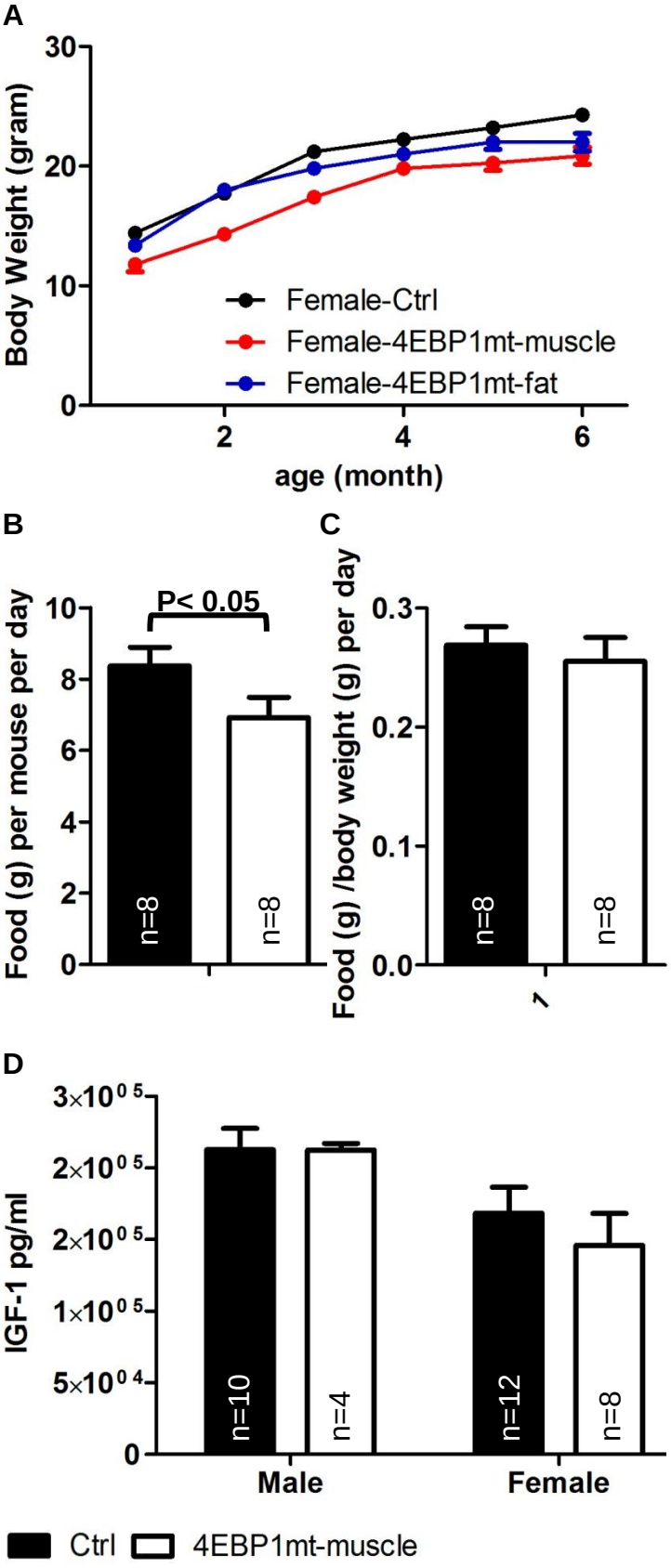

Supplementary Figure 4.

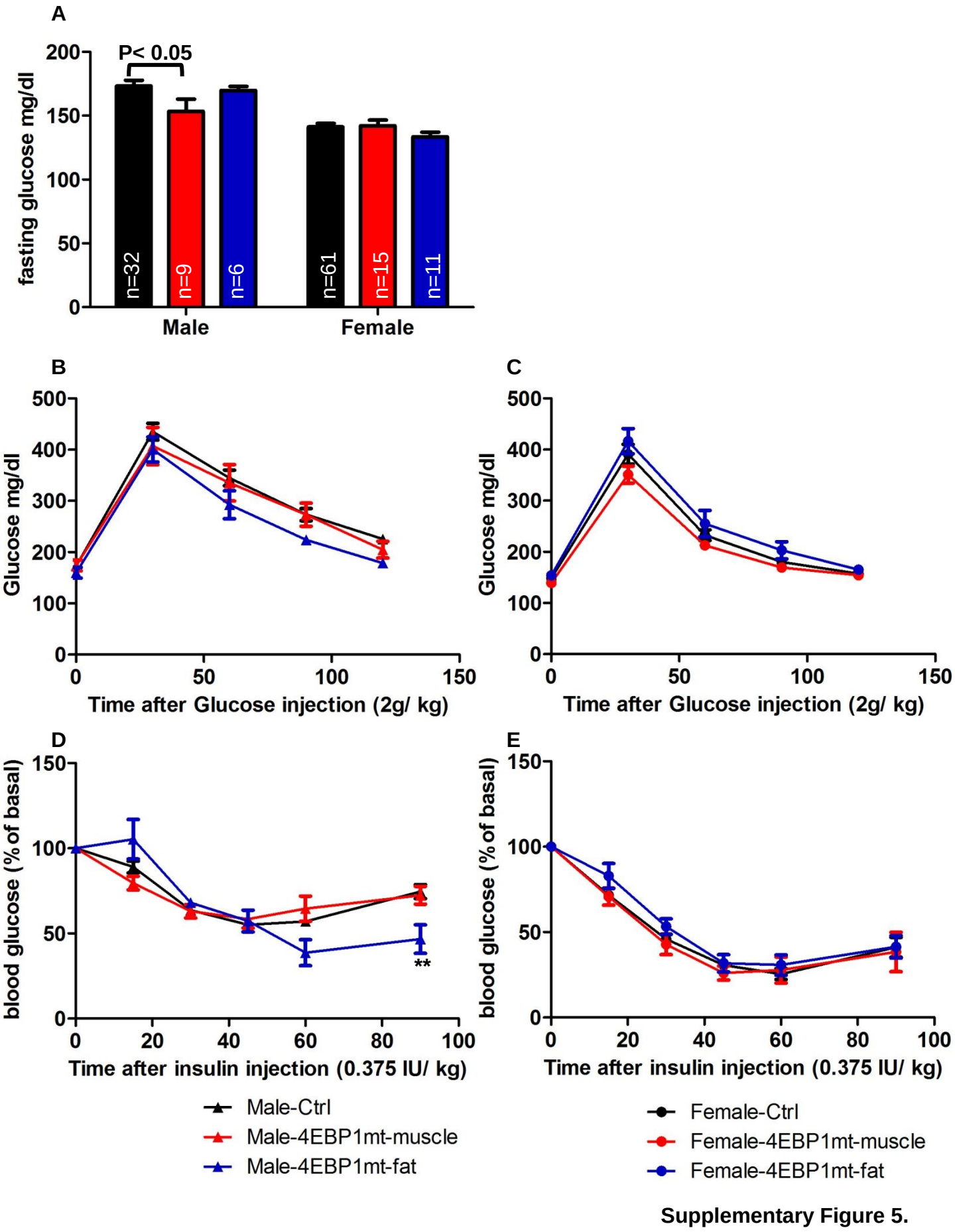

Supplementary Figure 5.

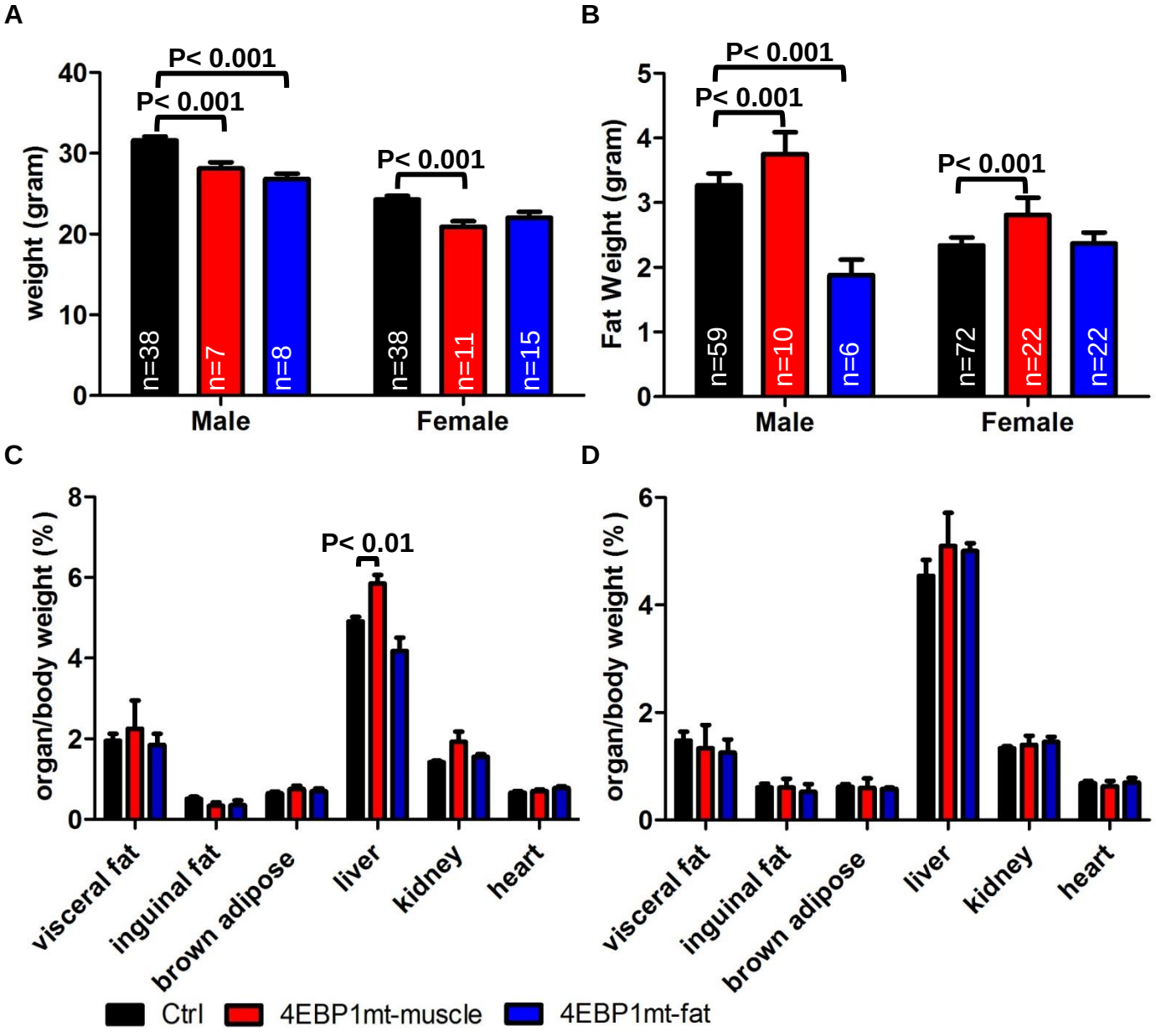

Supplementary Figure 6.

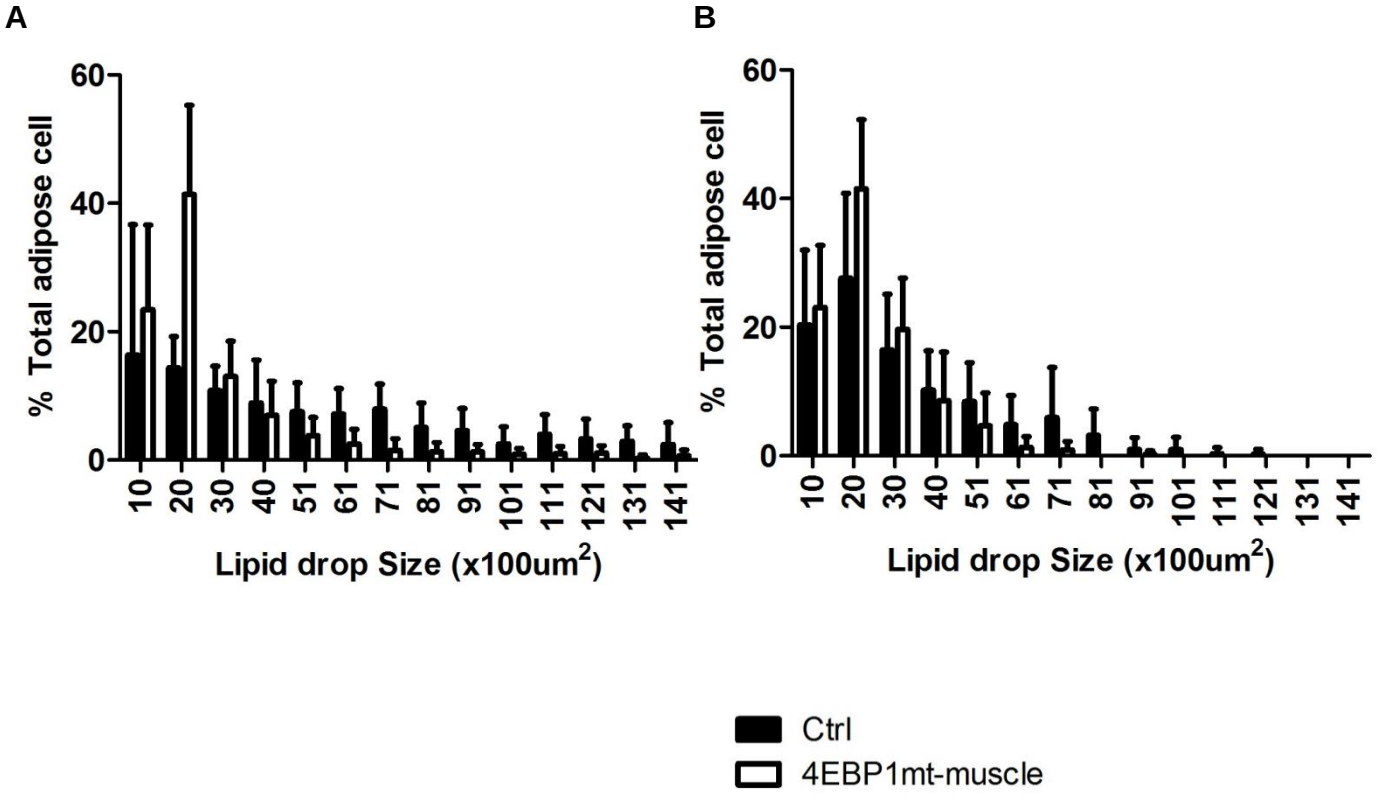

Supplementary Figure 7.

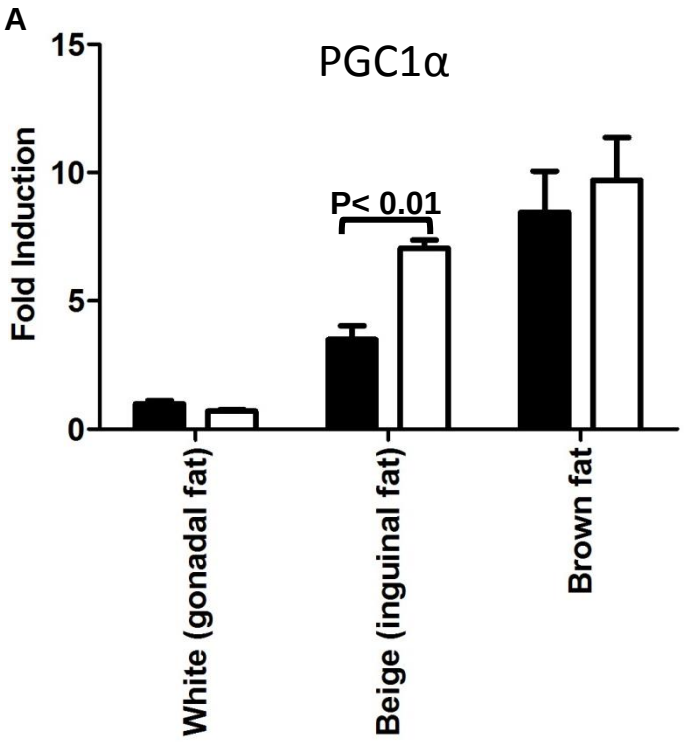

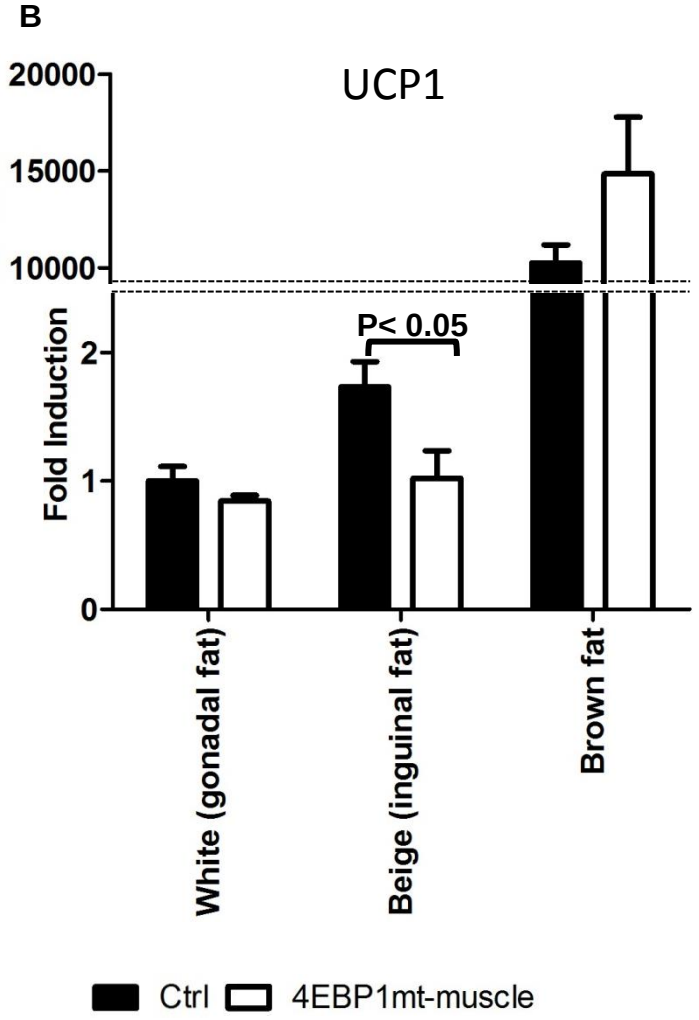

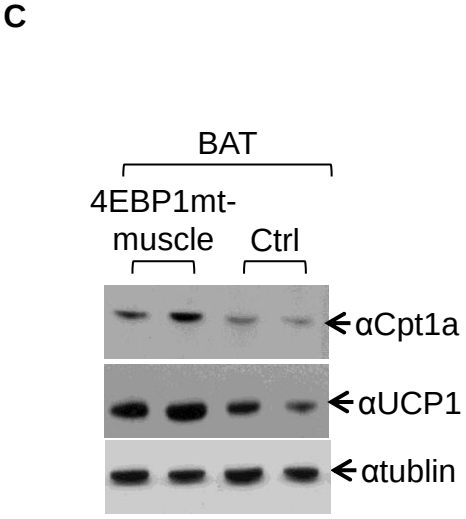

Supplementary Figure 8.

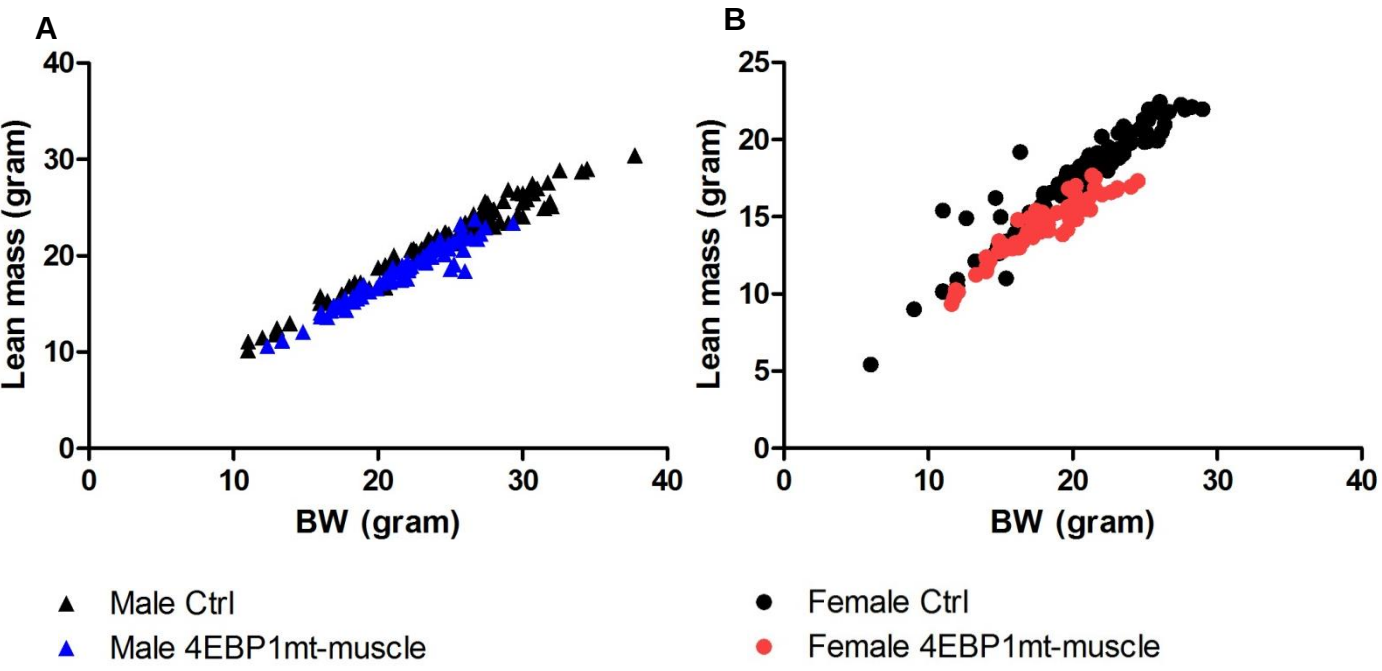

Supplementary Figure 9.

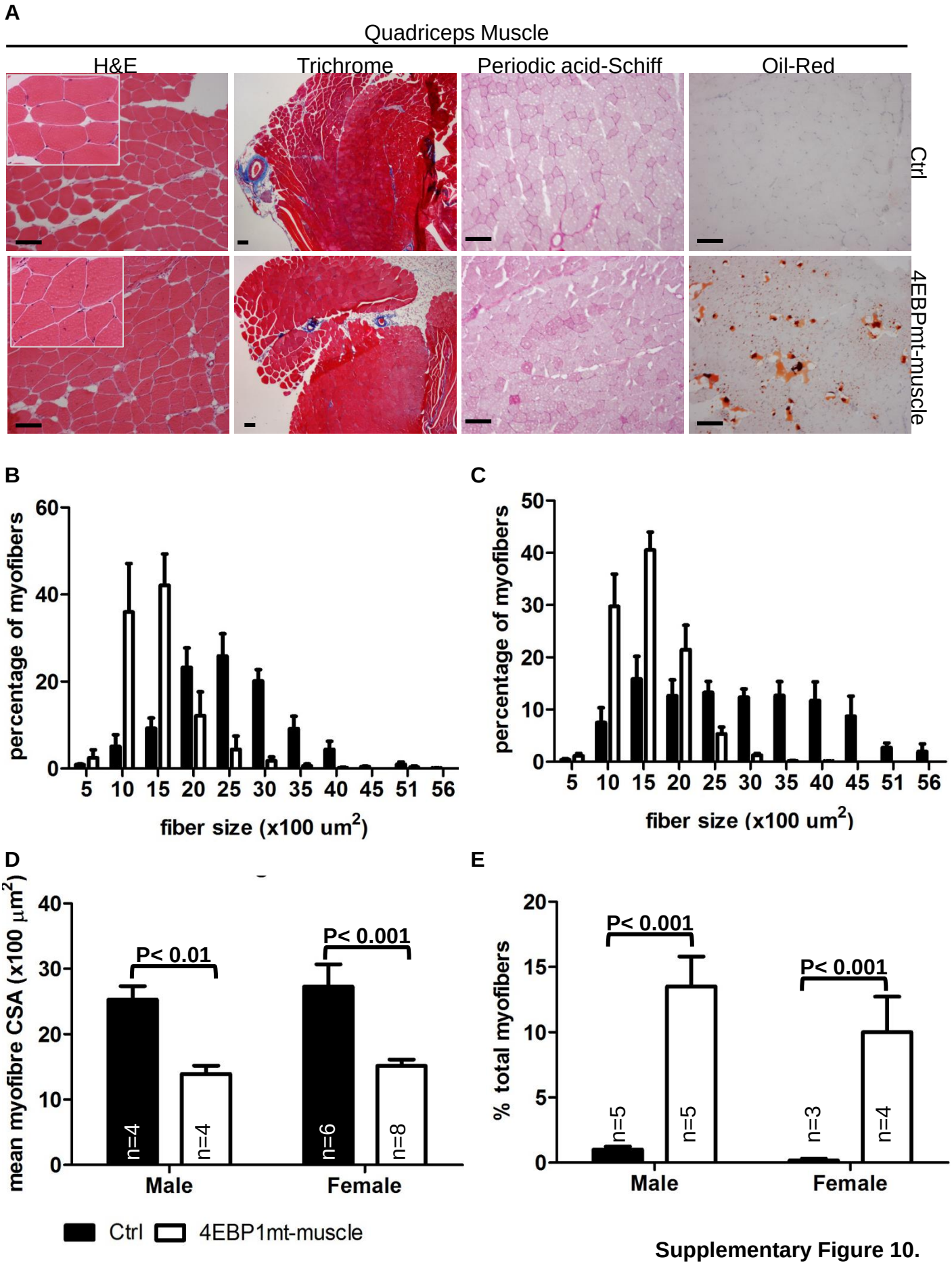

Supplementary Figure 10.

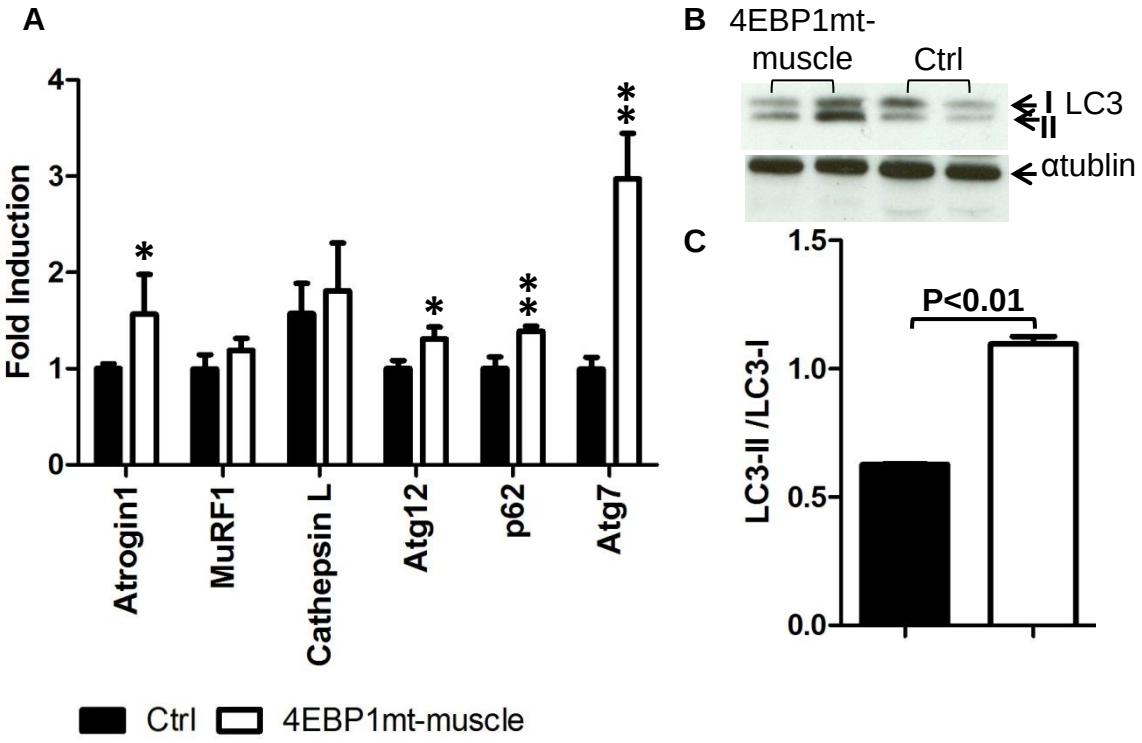

Supplementary Figure 11.

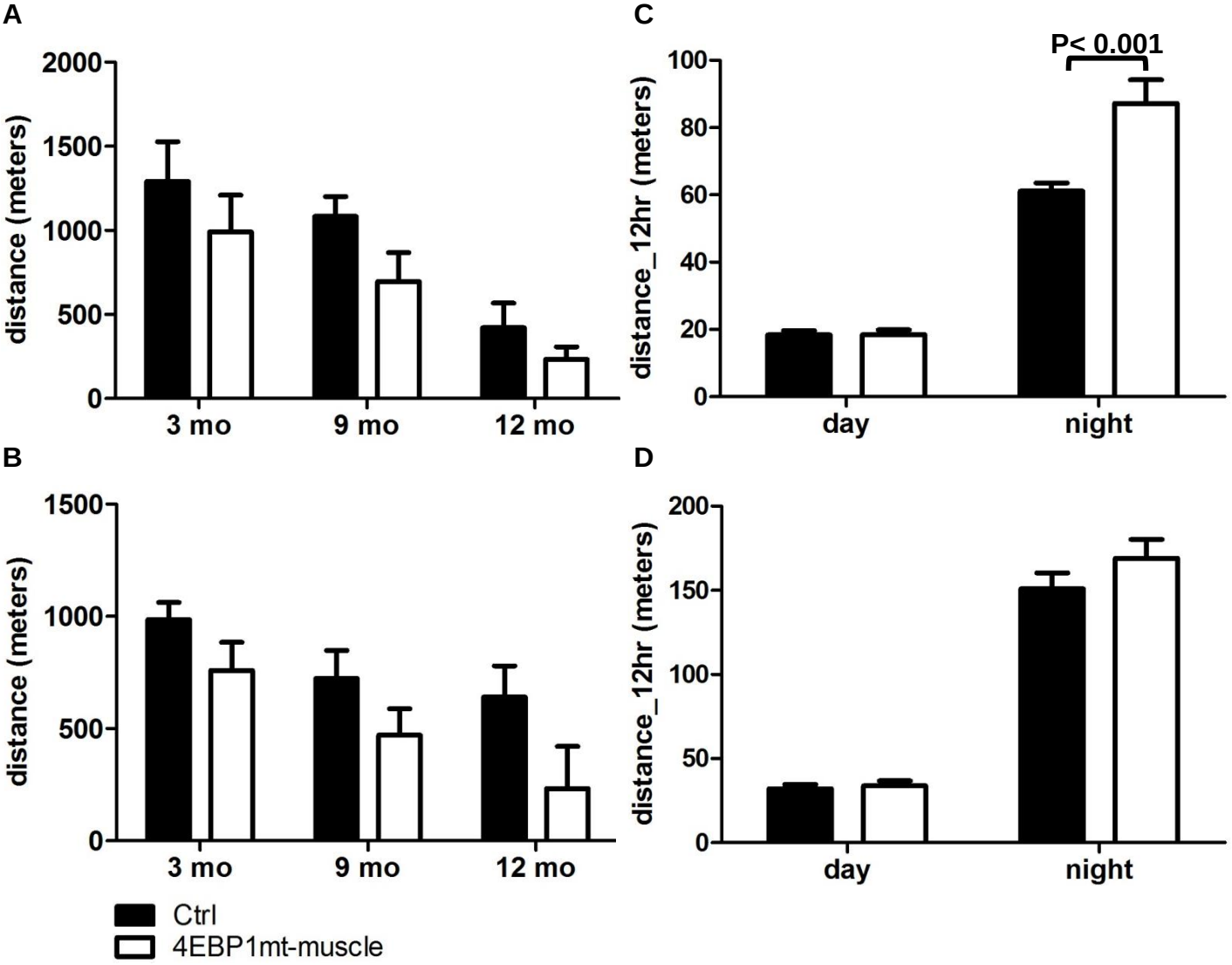

Supplementary Figure 12.

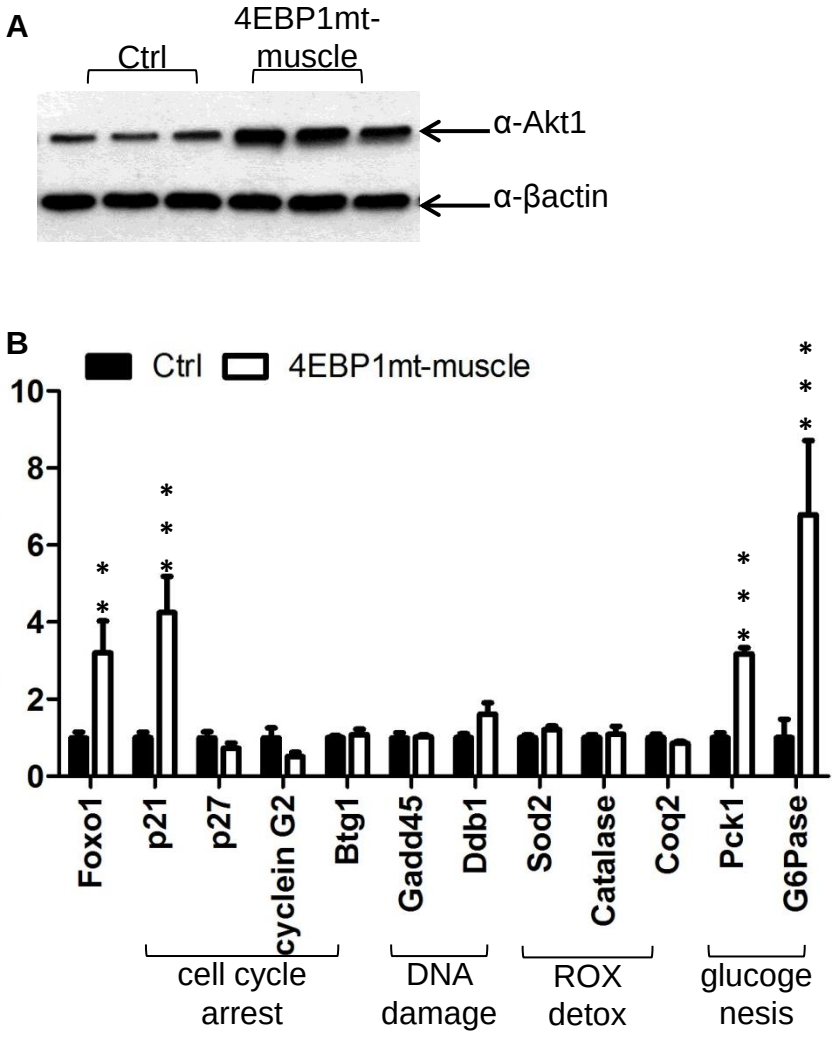

Supplementary Figure 13.

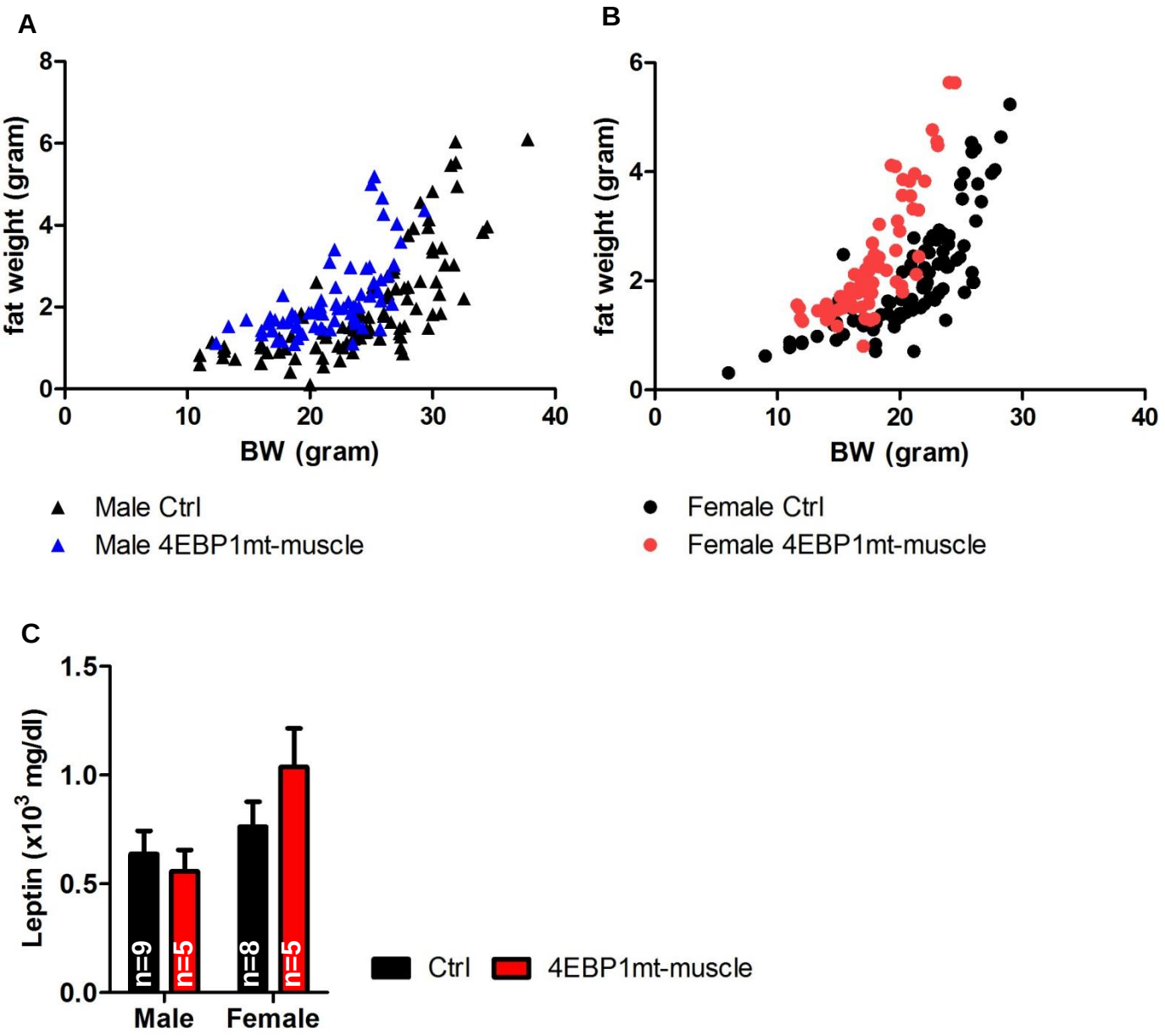

Supplementary Figure 14.

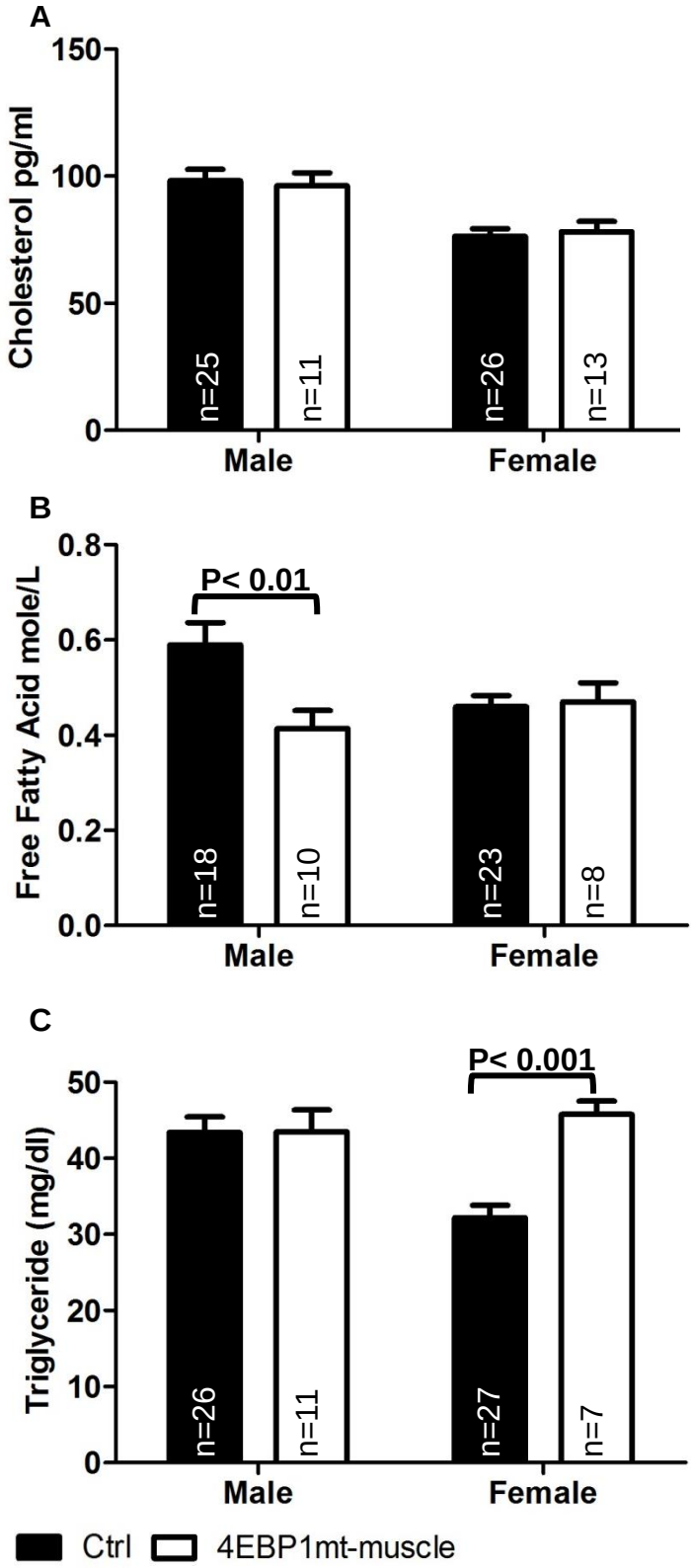

Supplementary Figure 15.

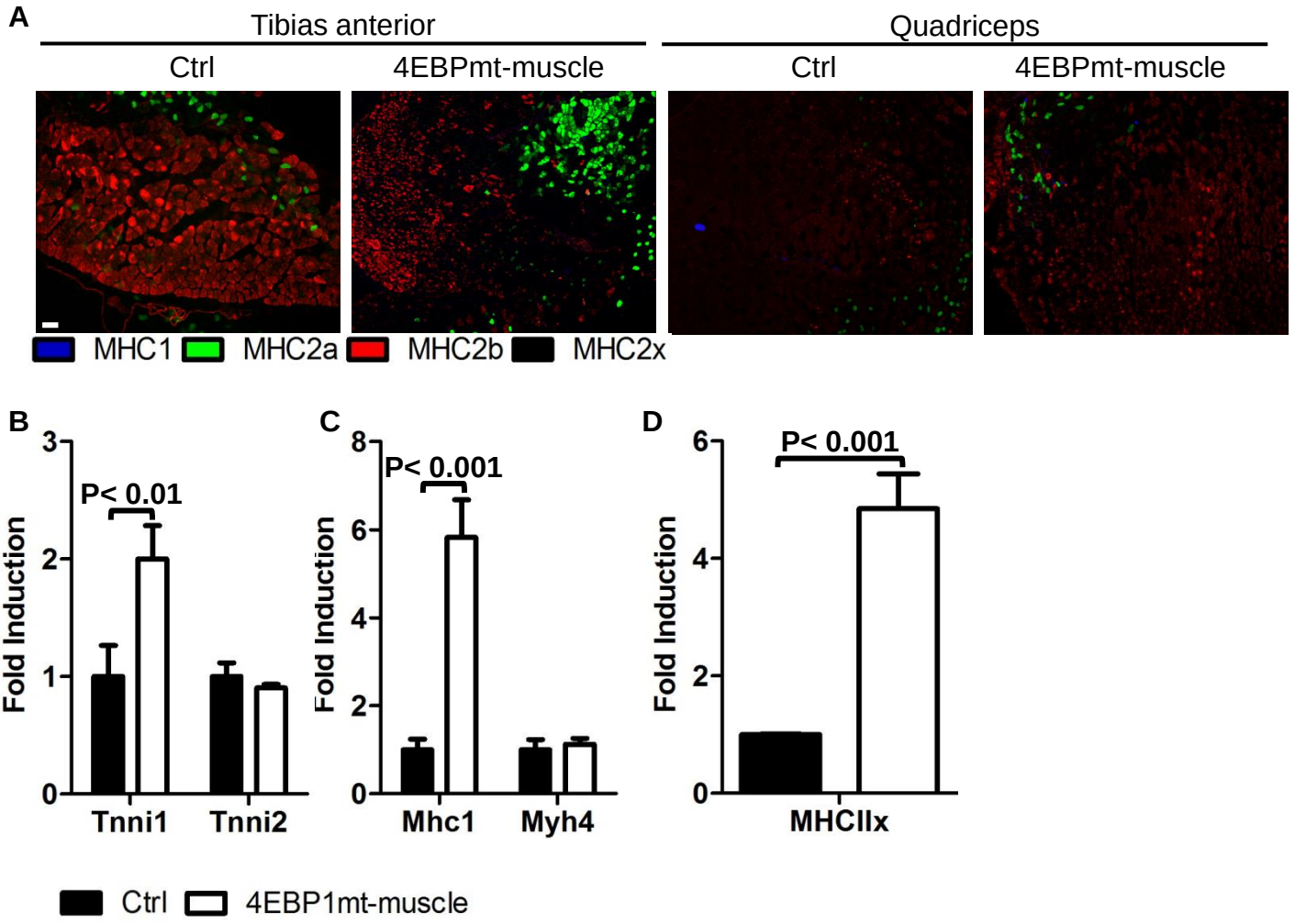

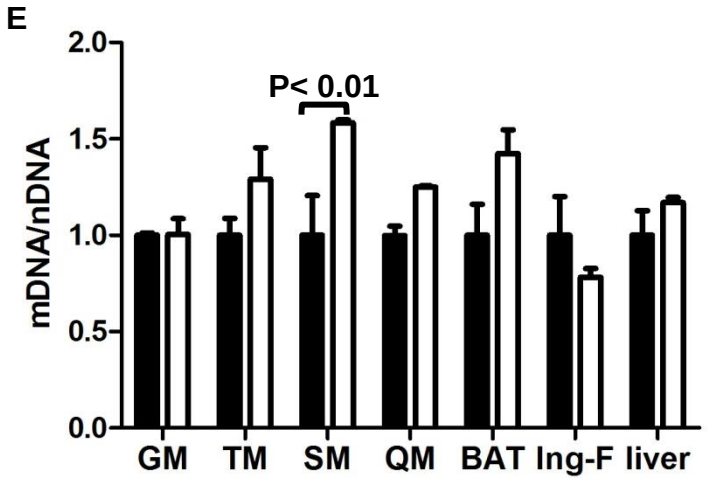

Supplementary Figure 16.

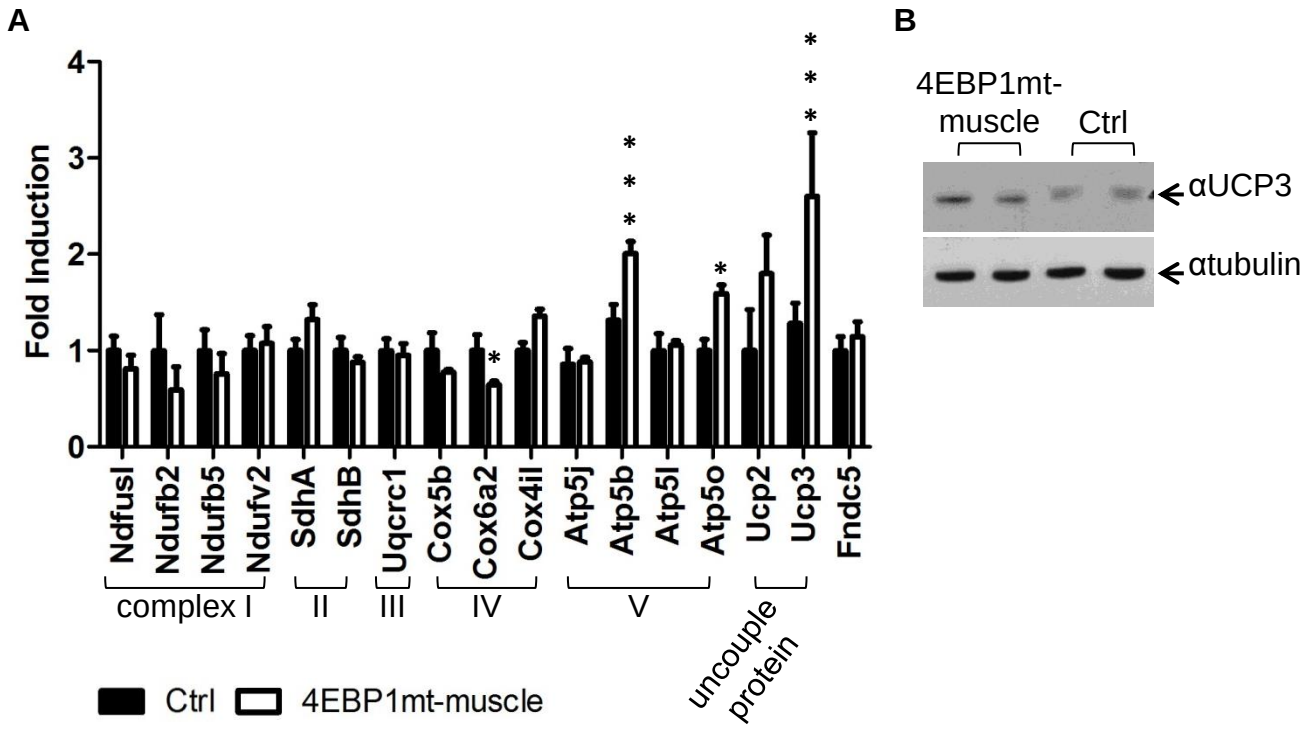

Supplementary Figure 17.

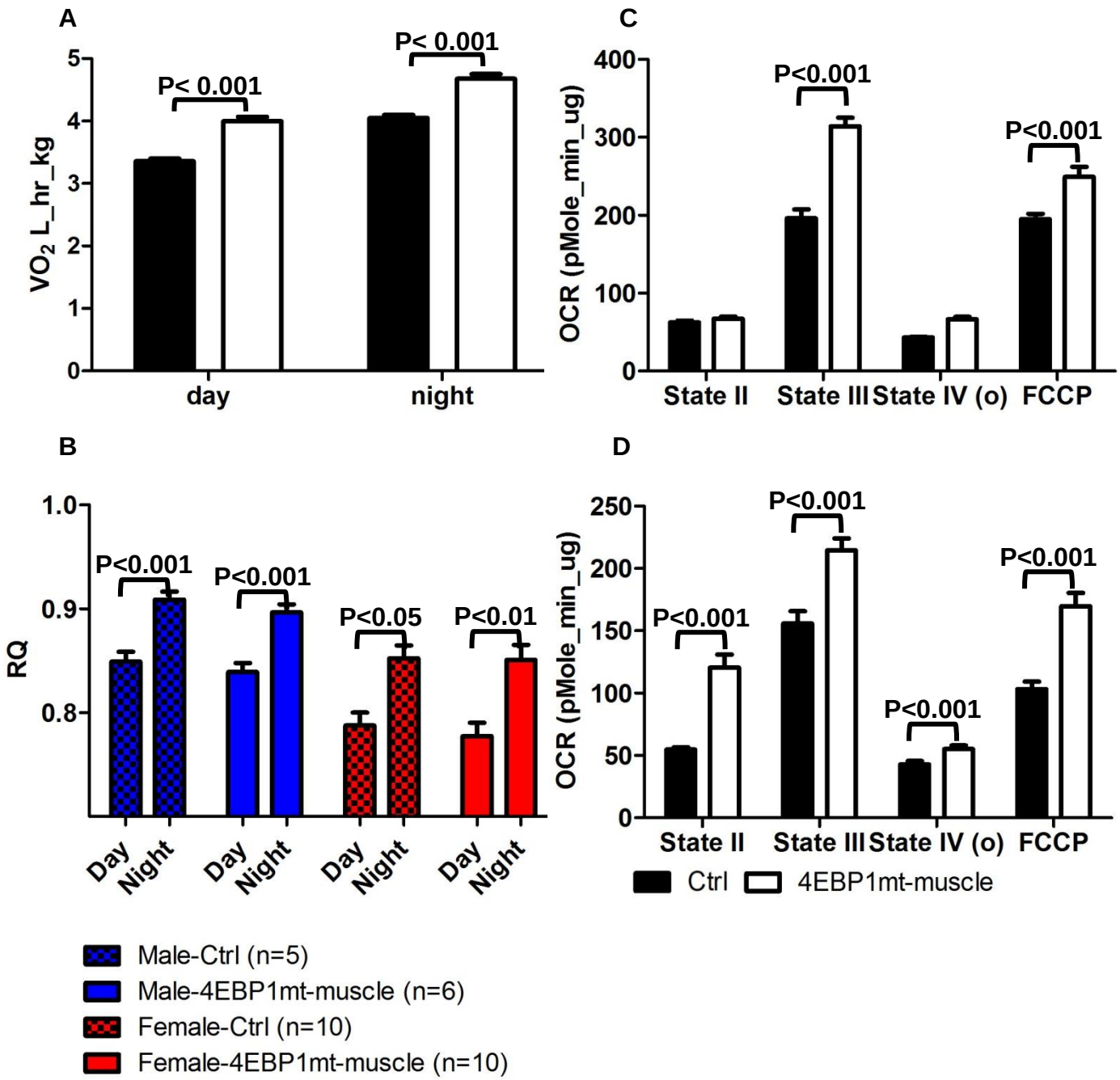

Supplementary Figure 18.

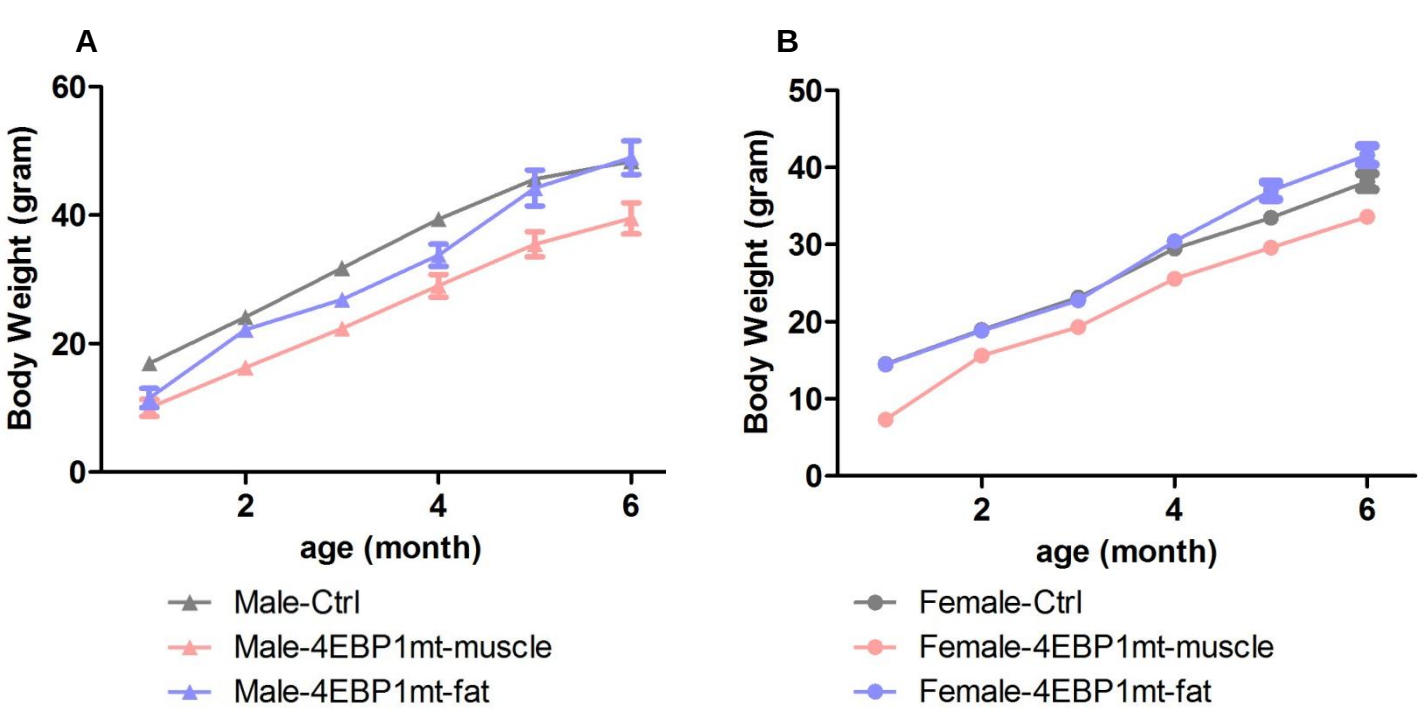

Supplementary Figure 19.

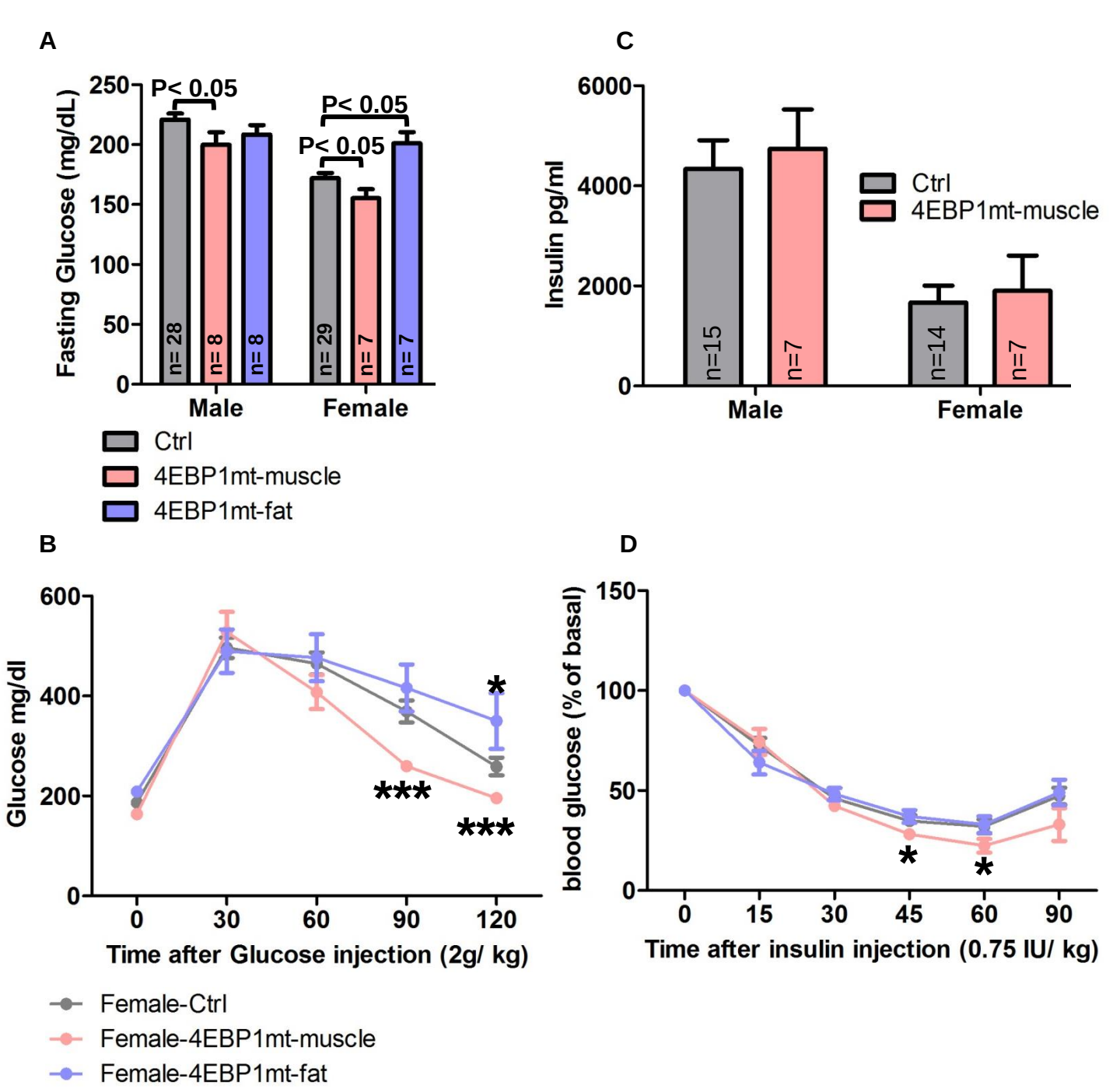

Supplementary Figure 20.

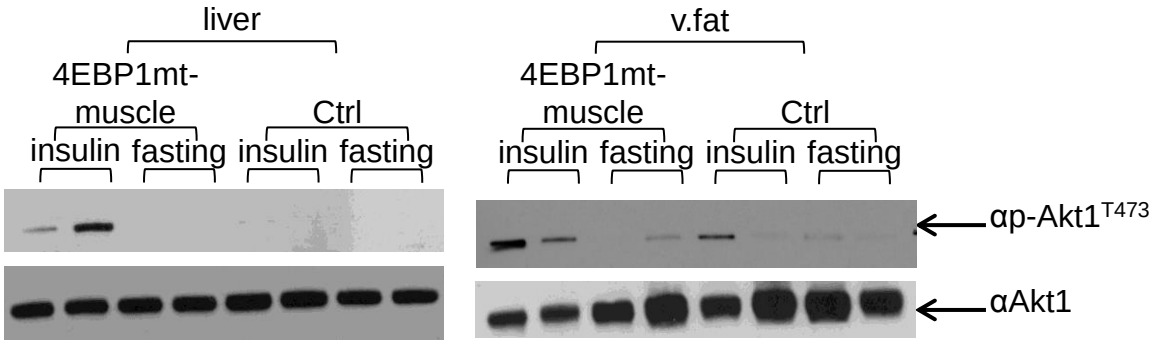

Supplementary Figure 21.

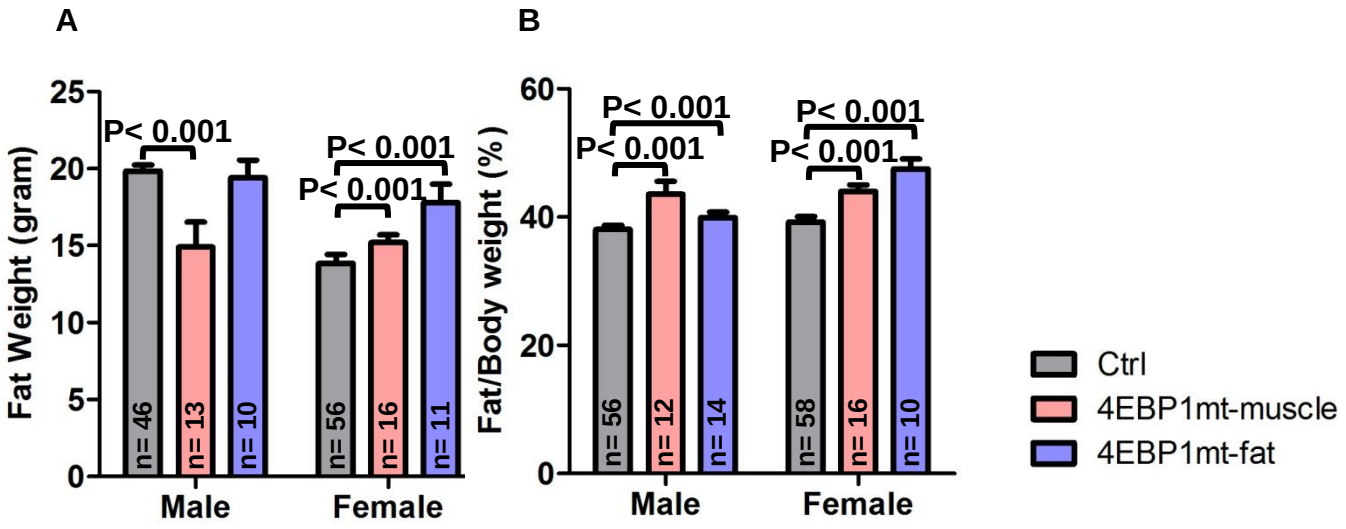

Supplementary Figure 22.

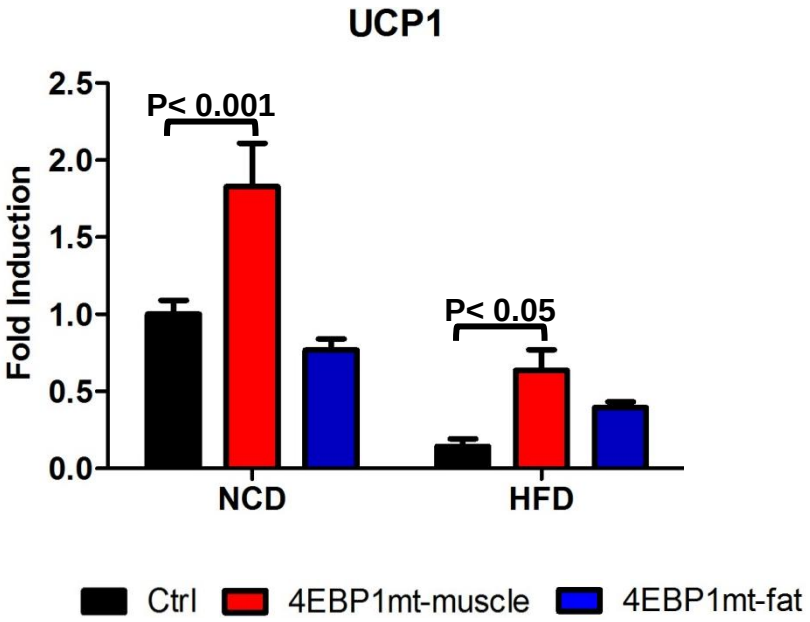

Supplementary Figure 23.

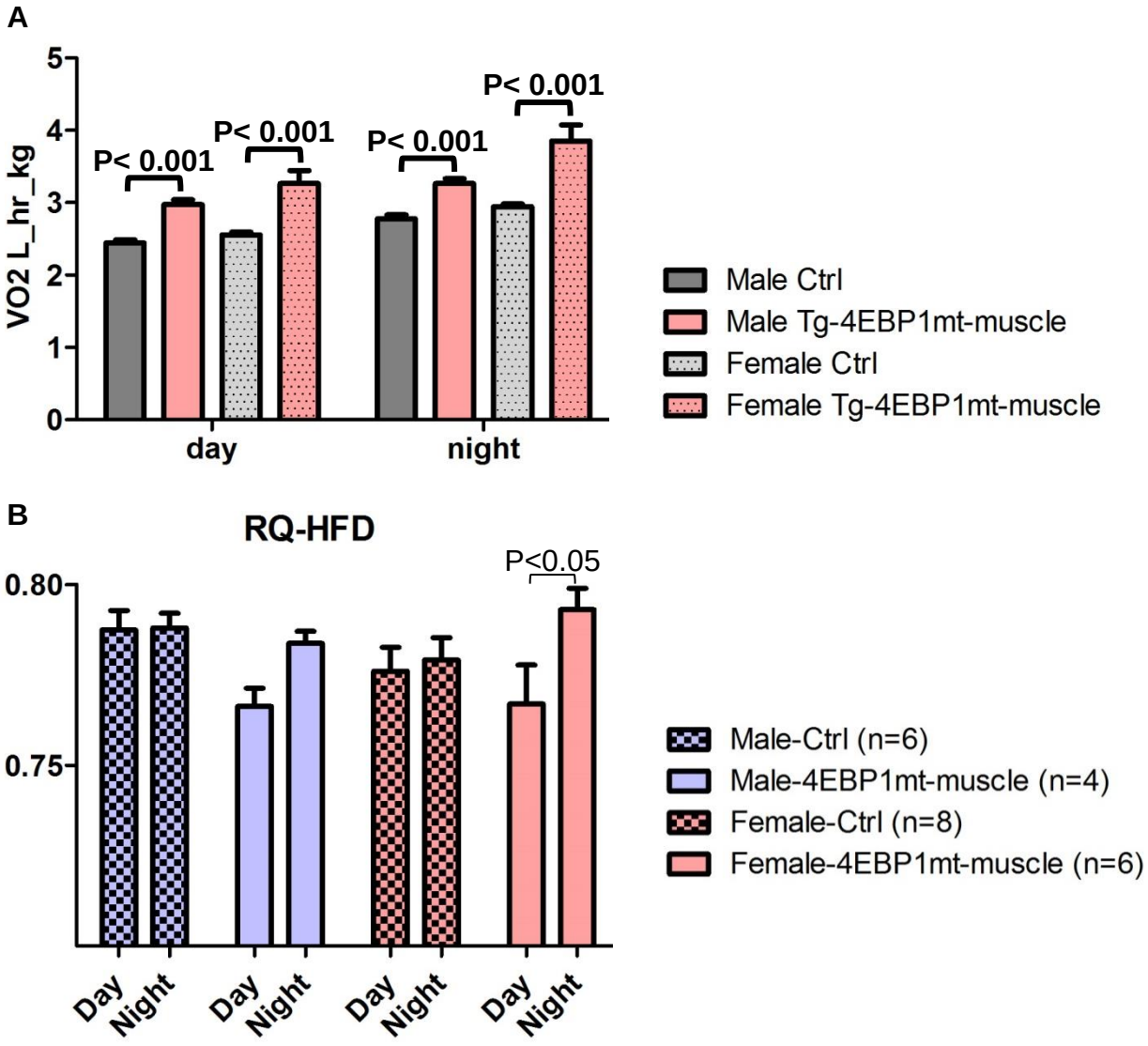

Supplementary Figure 24.

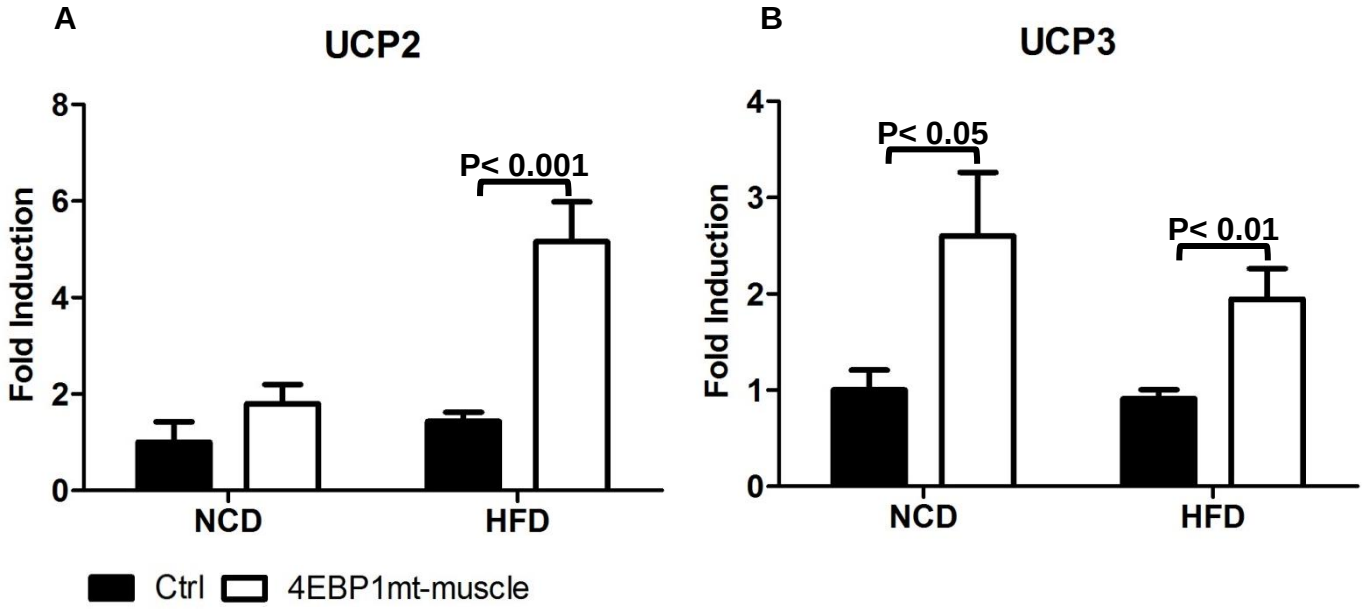

Supplementary Figure 25.

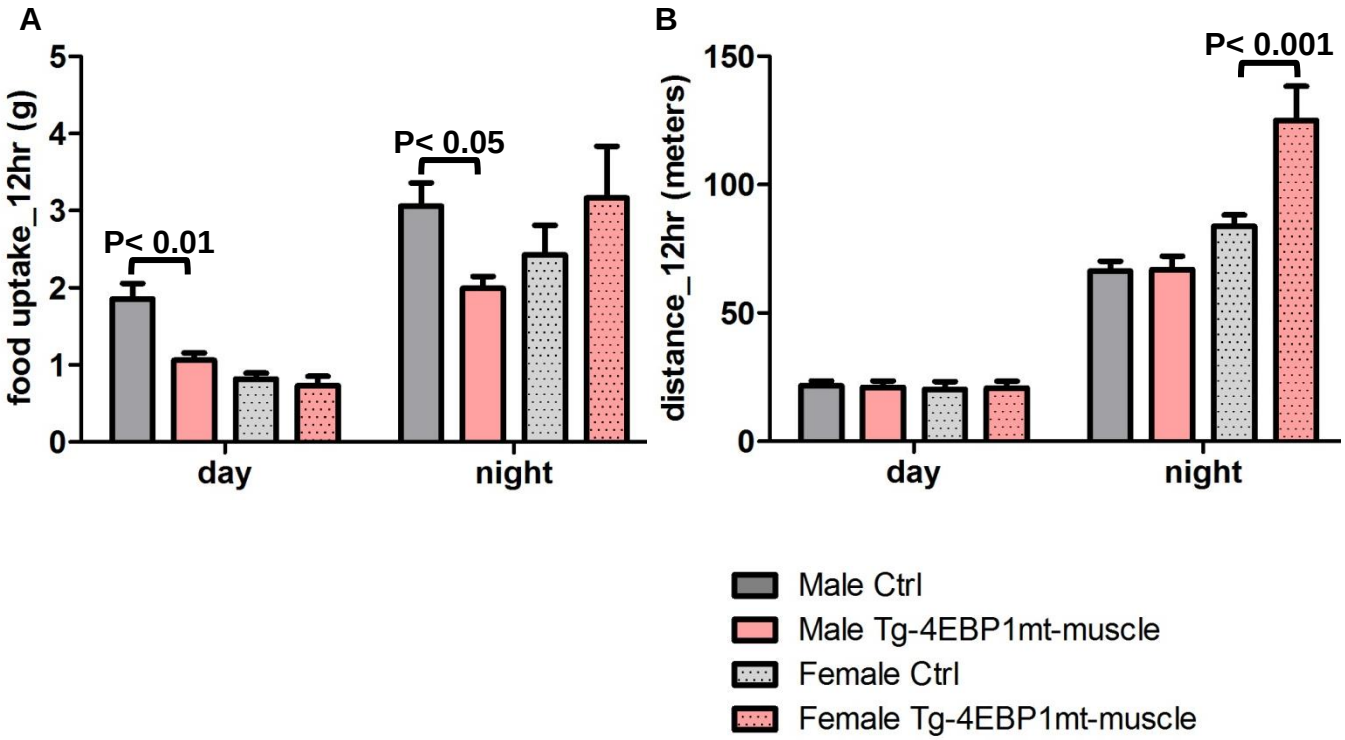

Supplementary Figure 26.

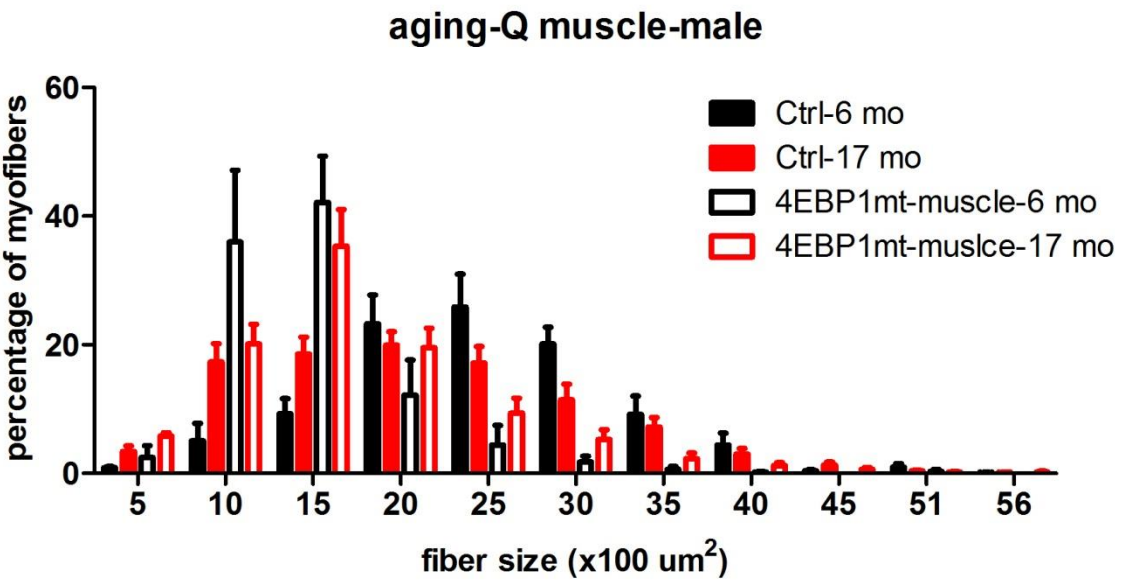

Supplementary Figure 27

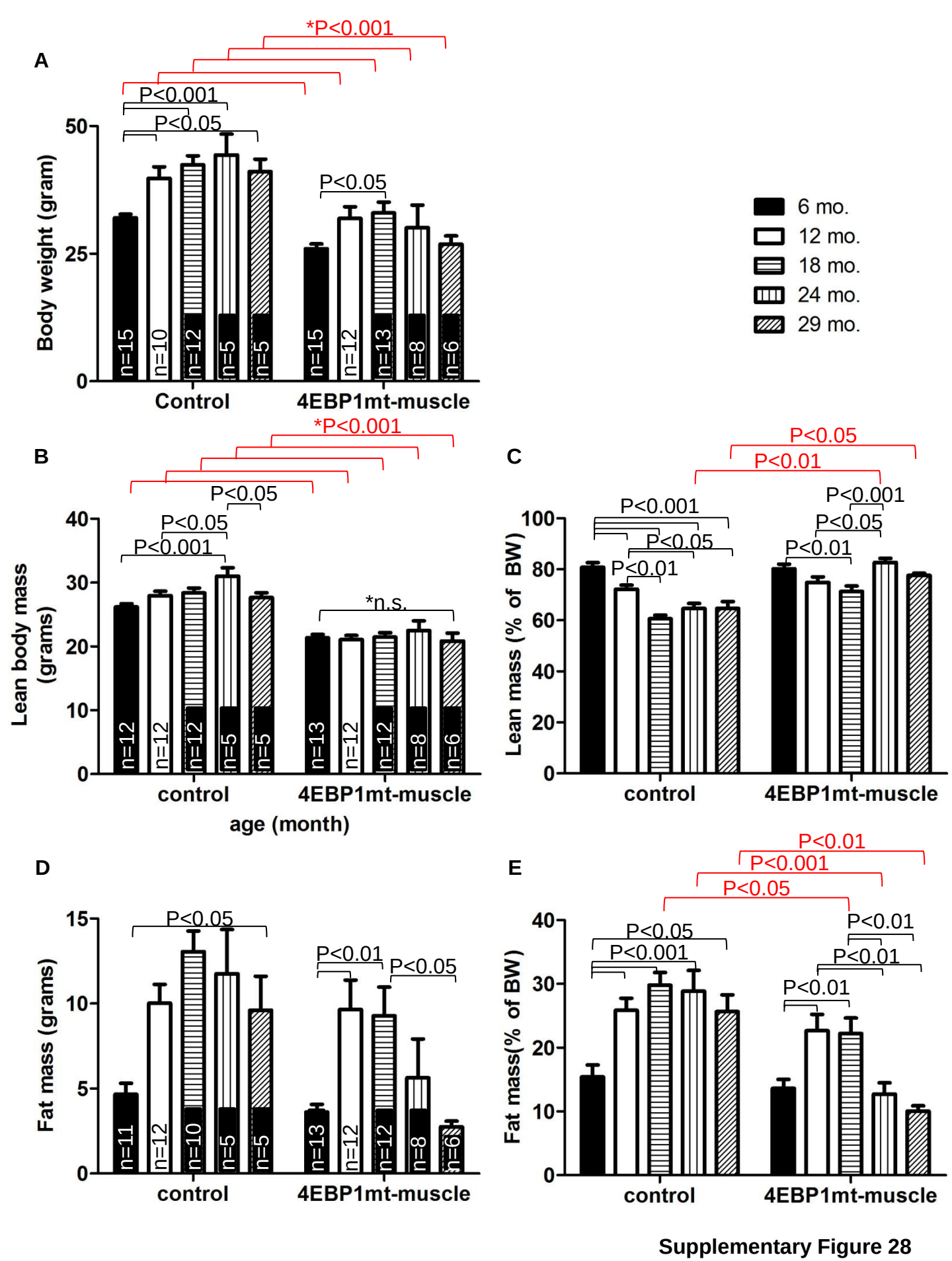

Supplementary Figure 28

A

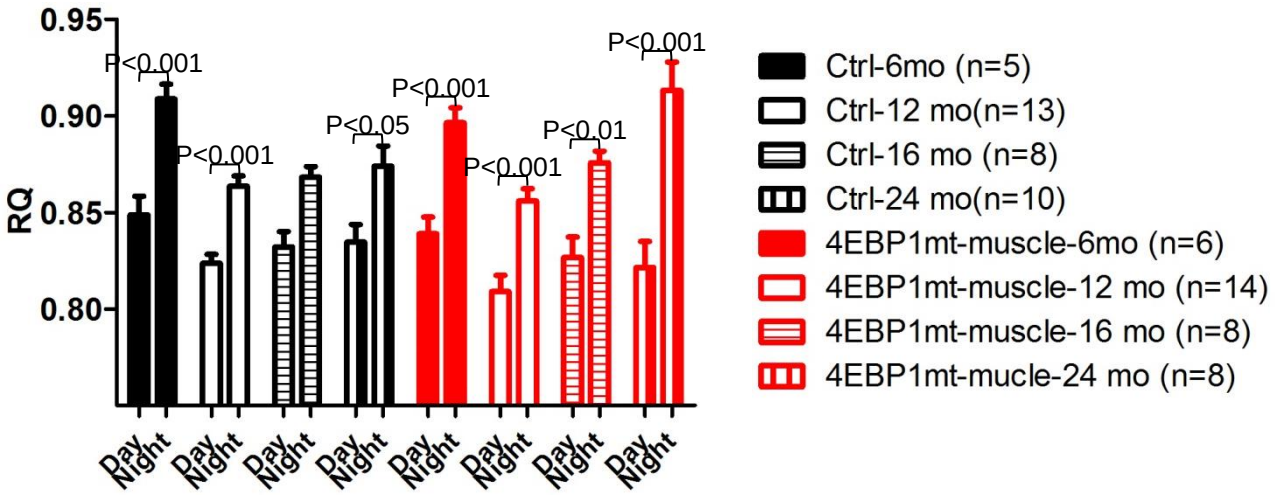

B

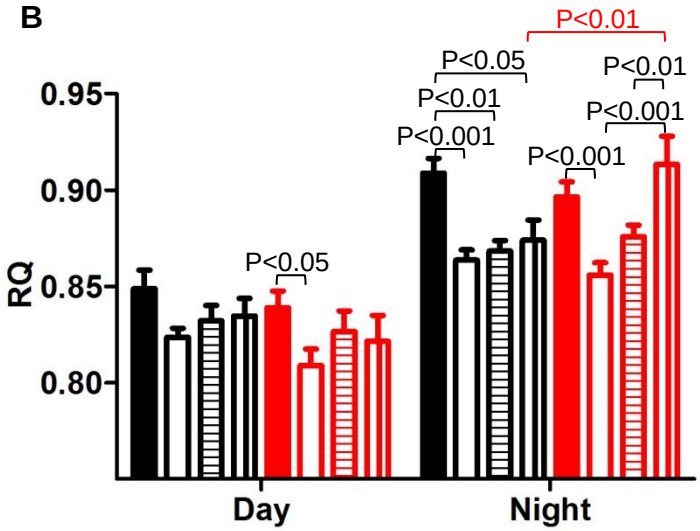

Supplementary Figure 29

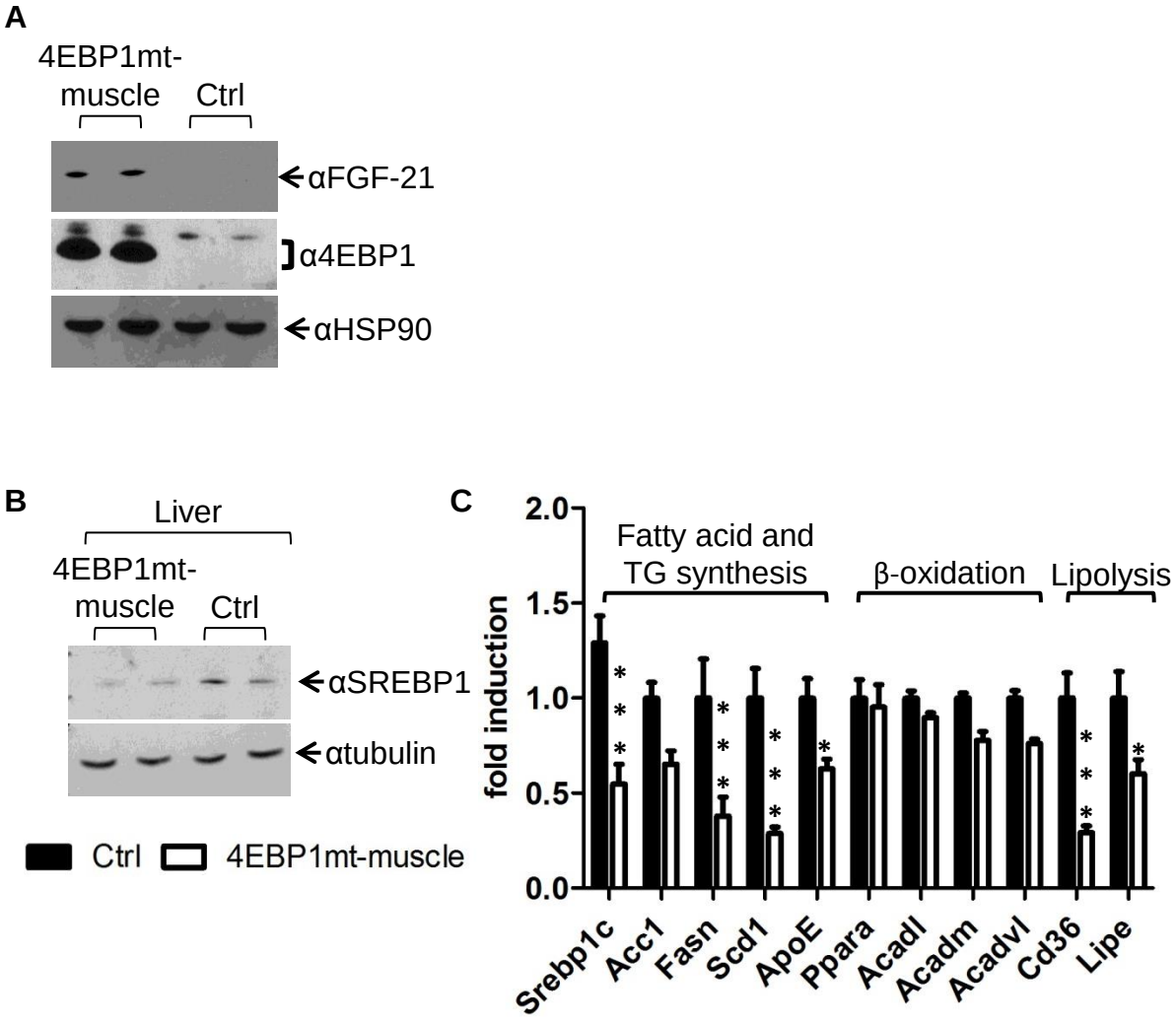

Supplementary Figure 30

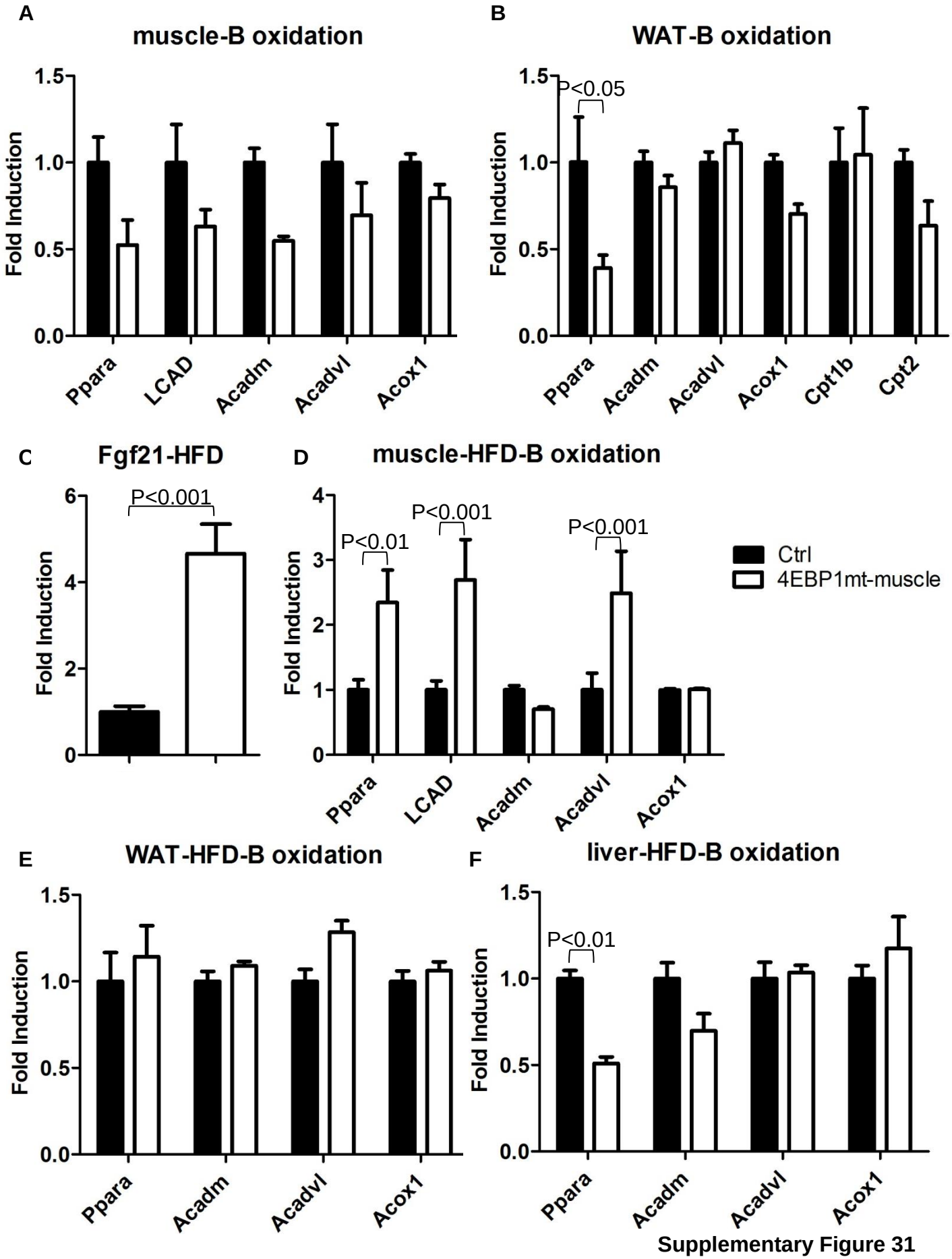

Supplementary Figure 31

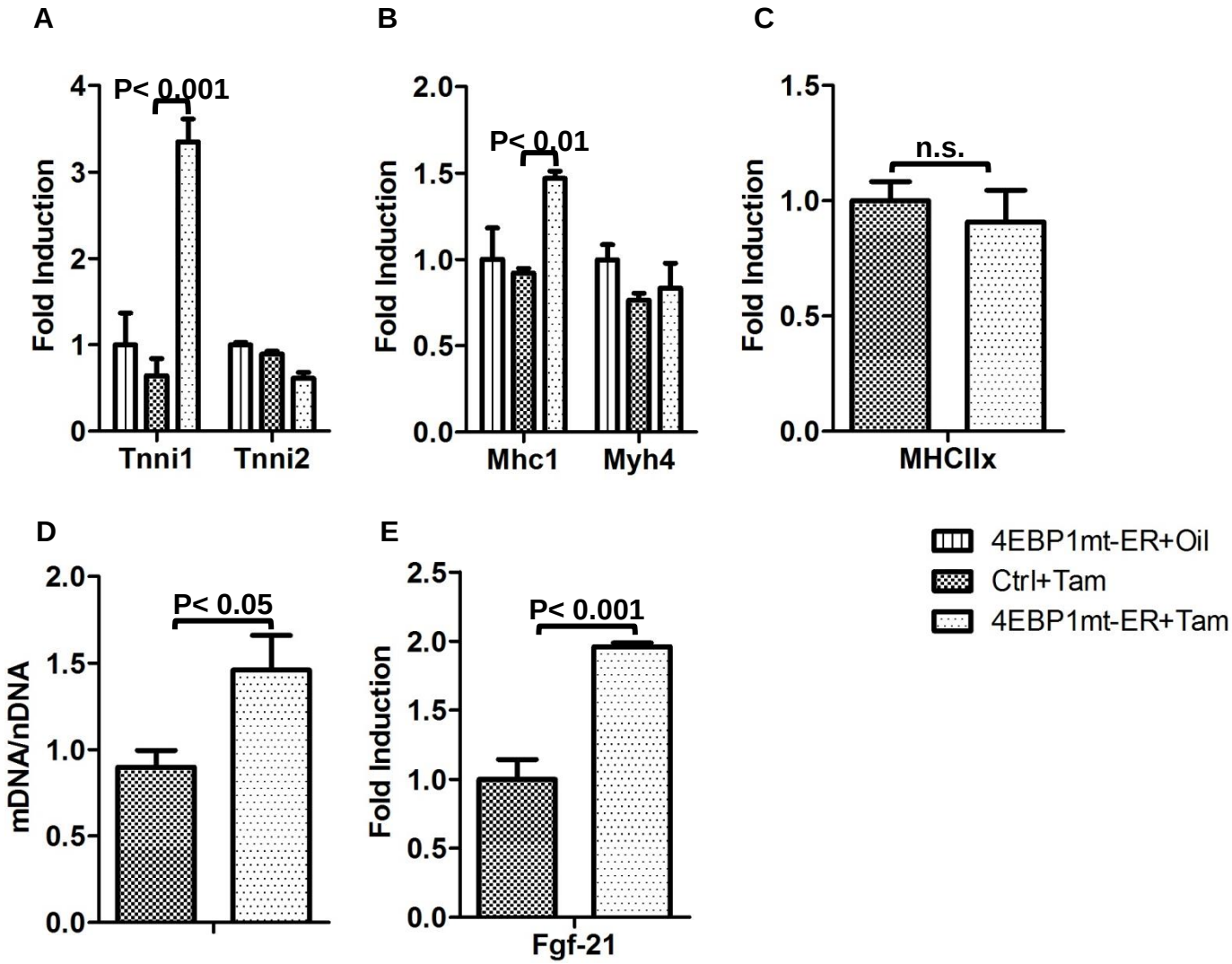

Supplementary Figure 32